The Journal of Experimental Biology 205, 939–958 (2002)
Printed in Great Britain © The Company of Biologists Limited
JEB3922

Kinematics of the buccal mass during swallowing based on magnetic resonance imaging in intact, behaving *Aplysia californica*

David M. Neustadter[1,2], Richard F. Drushel[3] and Hillel J. Chiel[1,3,4,*]

[1]*Department of Biomedical Engineering, Case Western Reserve University, Cleveland, OH 44106-7080, USA,* [2]*MR Systems Department, G. E. Medical Systems Israel Ltd, Keren Hayesod Street, PO Box 2071, Tirat Carmel 39120, Israel,* [3]*Department of Biology* and [4]*Department of Neurosciences, Case Western Reserve University, Cleveland, OH 44106-7080, USA*

*Author for correspondence at address 3 (e-mail: hjc@po.cwru.edu)

Accepted 14 January 2002

Summary

A novel magnetic resonance imaging interface has been developed that makes it possible to image movements in intact, freely moving subjects. We have used this interface to image the internal structures of the feeding apparatus (i.e. the buccal mass) of the marine mollusc *Aplysia californica*. The temporal and spatial resolution of the resulting images is sufficient to describe the kinematics of specific muscles of the buccal mass and the internal movements of the main structures responsible for grasping food, the radula and the odontophore. These observations suggest that a previously undescribed feature on the anterior margin of the odontophore, a fluid-filled structure that we term the prow, may aid in opening the jaw lumen early in protraction. Radular closing during swallowing occurs near the peak of protraction as the radular stalk is pushed rapidly out of the odontophore. Retraction of the odontophore is enhanced by the closure of the lumen of the jaws on the elongated odontophore, causing the odontophore to rotate rapidly towards the esophagus. Radular opening occurs after the peak of retraction and without the active contraction of the protractor muscle I2 and is due, in part, to the movement of the radular stalk into the odontophore. The large variability between responses also suggests that the great flexibility of swallowing responses may be due to variability in neural control and in the biomechanics of the ingested food and to the inherent flexibility of the buccal mass.

Key words: feeding, mollusc, biomechanics, *Aplysia californica*, magnetic resonance imaging, freely moving subject, behaviour.

Introduction

Adaptive behavior emerges from the interactions between the nervous system, the body and the environment (Chiel and Beer, 1997). Since certain aspects of adaptive behavior may not be observed unless all these components are interacting, it would be optimal to analyze them simultaneously and non-invasively. Given the limitations of current techniques for non-invasively monitoring neural and muscular activity, it is necessary to approximate simultaneous analysis. One effective approach has been the development of semi-intact preparations, in which it is possible to observe components of the behavior of interest while monitoring and manipulating the activity of neurons and muscles (Selverston, 1985; Stein et al., 1997). It has been possible to develop relatively non-invasive monitors of neural activity in intact humans performing motor, sensory and cognitive tasks (Cabeza and Nyberg, 2000; D'Esposito, 2000; Kuhtz-Buschbeck et al., 2001), of surface electromyographic activity in intact humans during behavior (Clarys, 2000; Grasso et al., 1998; Hatzitaki and McKinley, 2001) or of heart movements in intact humans at rest (Hardy et al., 1998). In this paper, we report the first application of a non-invasive technique for monitoring the internal muscular movements of a freely behaving subject whose neural control is also tractable to detailed neural analysis, another step towards simultaneous monitoring of all the components of adaptive behavior.

We have focused our study on molluscan feeding behavior. Feeding behavior has been intensively studied in a wide variety of molluscan species. A recent review describes the analysis of the movements of the feeding musculature and its neural control in a variety of molluscan genera, including *Lymnaea*, *Planobarius*, *Helisoma*, *Clione*, *Limax*, *Navanax*, *Pleurobranchaea* and *Tritonia* (Murphy, 2001). The subject that we have chosen, the marine mollusc *Aplysia californica*, has been intensively studied as a model system for understanding the neural basis of learning, memory and motivated behaviors. The neural, biophysical and molecular mechanisms of learning and memory identified in *Aplysia californica* have served as the basis for understanding the molecular mechanisms of learning in mammals and primates (Kandel and Pittenger, 1999; Silva et al., 1998). Feeding behavior in *Aplysia californica* has also been

intensively studied as a model system for understanding the modulation of behavior under the control of motivational variables (Kupfermann, 1974; Kupfermann et al., 1998). Many of the motor neurons controlling the feeding apparatus, the buccal mass, have been identified (Church et al., 1991; Church and Lloyd, 1994; Morton and Chiel, 1993), as have the interneurons that play a critical role in pattern generation and in switching among different feeding responses, such as biting, swallowing and rejection (Evans and Cropper, 1998; Hurwitz et al., 1994, 1966, 1997; Hurwitz and Susswein, 1996; Jing and Weiss, 2001; Kirk, 1989; Rosen et al., 1991; Susswein and Byrne, 1988).

Analysis of the biomechanics of feeding in *Aplysia californica* has recently become a focus of interest. Earlier studies demonstrated that the feeding musculature was subject to both extrinsic and intrinsic modulatory influences (for a review, see Katz and Frost, 1996) (see also Morgan et al., 2000). The implications of these modulatory influences for rhythmic behavior that must occur at different speeds, and for the integration of signals released at different frequencies of neural activation, have been explored (Brezina et al., 2000; Weiss et al., 1992). The potentially context-dependent role of a specific muscle, the I5 or ARC muscle, has been examined in isolated buccal masses using ultrasound and intracellular stimulation of the motor neurons controlling the muscle (Orekhova et al., 2001). A detailed Hill-type model of a muscle of the buccal mass, the I2 muscle, has recently been described on the basis of measurements of its force/frequency, length/tension, force/velocity and passive properties (Yu et al., 1999). Furthermore, the kinematics of the buccal mass as a whole has been characterized in juvenile transilluminated animals (Drushel et al., 1997) and has served as the basis for kinematic models (Drushel et al., 1998). The previous work in transilluminated juveniles indicated that the buccal mass assumed characteristic shapes during different parts of the swallowing cycle, but the movements of the internal musculature responsible for these shapes was not clear.

To visualize the kinematics of the buccal musculature in intact, behaving animals in the mid-sagittal plane, which provides maximal information about the internal structures, we have developed a novel magnetic resonance imaging (MRI) interface that makes it possible to obtain an intrinsic reference frame for structures in freely moving subjects and have developed an apparatus in which freely behaving *Aplysia californica* can feed and be imaged simultaneously. Studying the kinematics of the buccal mass in intact animals makes it possible to determine the movements of its internal musculature within their natural context of sensory feedback and mechanical interaction with the environment. We report that it is possible directly to monitor the kinematics of individual muscles and the coordinated movements of many structures of the buccal mass using this technique, and these kinematic measurements clarify many aspects of the muscular mechanisms of swallowing in *Aplysia californica*. Portions of this work have appeared in preliminary form (Chiel et al., 1999; Neustadter et al., 2001; Sutton et al., 2000).

Materials and methods

Magnetic resonance imaging of feeding in vivo

Obtaining magnetic resonance images with high temporal resolution of swallowing in intact, behaving animals required the development of a novel real-time MRI interface, an appropriate tank and coil, and a feeding stimulus that would ensure reliable swallowing movements over several minutes.

Real-time MRI interface

A novel interface was developed to address two potential problems of imaging freely moving subjects: (i) it is essential to maintain accurate localization as an animal moves, and (ii) it is essential to assess the degree of error in the mid-sagittal image, which could be para-sagittal or rotated along the antero-posterior, dorso-ventral or medio-lateral axes. To address both these concerns, the interface acquires three interleaved orthogonal images. Acquiring three orthogonal images provides a rapidly updated reference frame intrinsic to the moving subject. Furthermore, the two images orthogonal to the mid-sagittal slice make it possible to assess whether that image is para-sagittal or rotated. To minimize artifact in the main image due to intersection with the orthogonal slices, despite the long relaxation time (T_1) of sea water, the tip angles for the main mid-sagittal slice, and for the auxilliary coronal and axial slices are different (40 °, 10 ° and 10 °, respectively); for the theory underlying these choices, see (D. M. Neustadter and H. J. Chiel, in preparation). The time between repeated acquisitions of the main image was 310 ms, and the time between repeated acquisitions of each orthogonal image was 620 ms.

The user interface runs in two modes. In the localization mode, a new image is acquired every time the user modifies a scan parameter. In the dynamic imaging mode, acquisition runs continuously. Switching between the two modes takes less than 1 s, allowing dynamic imaging to be started immediately when the required slice is located and allowing relocalization to be performed immediately when subject movement is observed. Each image, whether a main image or an orthogonal image, is reconstructed immediately upon the completion of its acquisition and immediately displayed in the appropriate window of the user interface. In addition, a schematic representation of the orientation of the main slice is displayed, and the intersection of the main slice with the two orthogonal slices can be interactively modified by the user.

Data were acquired using echo planar imaging with standard two-dimensional Fourier transform reconstruction. The Elscint 2T-Prestige whole-body MRI system was used, with a 15 $mT\,m^{-1}$ maximum gradient strength and a 30 $mT\,m^{-1}\,ms^{-1}$ maximum slew rate, allowing 64 encodings with a 1 mm pixel resolution to be acquired in 155 ms. The resolution was 1 mm×1 mm pixels using a total acquisition matrix of 64×128. Details of the imaging sequence are shown in Fig. 1A.

Tank and coil for MRI of Aplysia californica

The imaging tank and coil are shown in Fig. 1B. The tank was long and cylindrical to avoid susceptibility artifacts. The

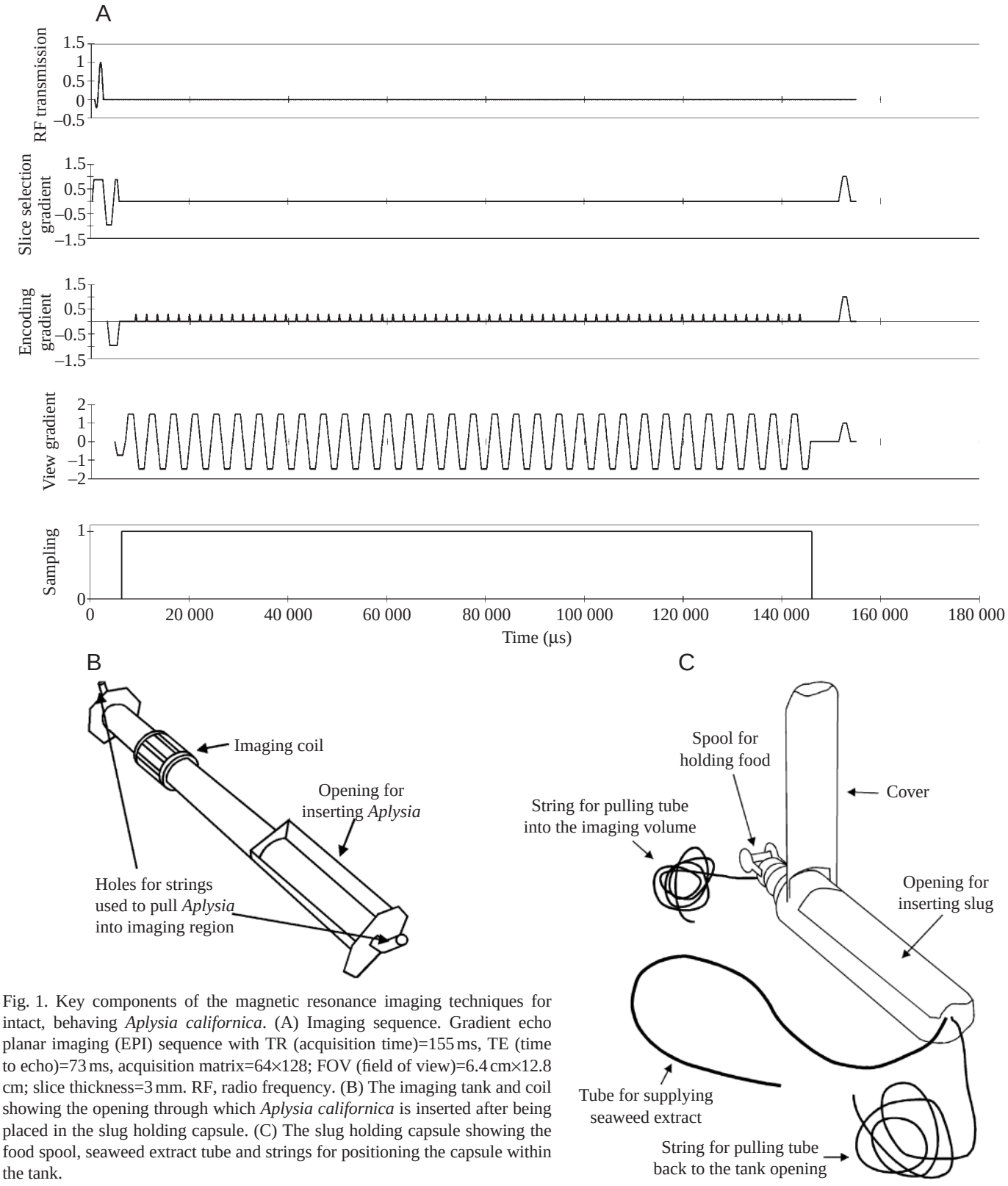

Fig. 1. Key components of the magnetic resonance imaging techniques for intact, behaving *Aplysia californica*. (A) Imaging sequence. Gradient echo planar imaging (EPI) sequence with TR (acquisition time)=155 ms, TE (time to echo)=73 ms, acquisition matrix=64×128; FOV (field of view)=6.4 cm×12.8 cm; slice thickness=3 mm. RF, radio frequency. (B) The imaging tank and coil showing the opening through which *Aplysia californica* is inserted after being placed in the slug holding capsule. (C) The slug holding capsule showing the food spool, seaweed extract tube and strings for positioning the capsule within the tank.

diameter of the tank also had to be smaller than or equal to the imaging field of view to avoid folding artifacts in the encoding direction because sea water produces a relatively high signal. The tank is 6.4 cm in diameter, allowing 64 1 mm pixels in the view direction with no folding, and 82 cm in length. The imaging coil is a standard transmit/receive quadrature birdcage coil whose dimensions were optimized to maximize signal-to-noise ratio and image uniformity. The coil is 12 cm in length

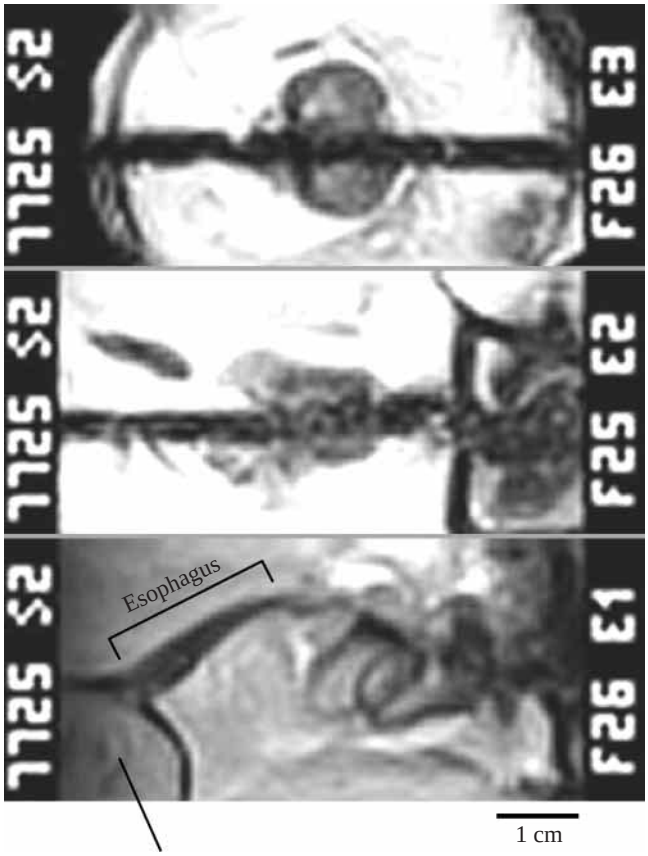

Fig. 2. Determining that the mid-sagittal image is correctly oriented. The mid-sagittal image is shown at the bottom. The right of the figure is anterior (the jaws of the animal) and left of the figure is posterior (the lumen of the gut and the esophagus are visible and labelled; this convention for positioning mid-sagittal images will be used throughout the paper). The coronal image that was recorded 155 ms before this mid-sagittal image is shown in the middle (right is anterior, left is posterior) and the axial image recorded 155 ms after this mid-sagittal image is shown at the top (left is dorsal, right is ventral). Note that the orthogonal images are both symmetrical and centered around the midline, providing evidence that the sagittal image is neither para-sagittal nor significantly rotated.

and 8 cm in diameter and is permanently attached to the imaging tank. The animal is placed inside a holding capsule (Fig. 1C), which is inserted into the tank, and the holding capsule is then pulled into the imaging region using strings that exit the tank at either end. The animals used in these imaging procedures were the largest that would fit in the holding capsule and tank (400–580 g) to maximize buccal mass size (approximately 2.5 cm×2 cm×2 cm).

Feeding stimulus

When fed a thin strip of seaweed, 400 g animals normally ingest it at a peak rate of approximately 0.5 cm s^{-1}. With the placement and imaging procedure taking up to 2–3 min, a strip of food close to 1 m in length is required to maintain steady swallowing responses. Most seaweed stipes are not that long or are too fragile to be cut into long strips. Instead, we used seaweed-flavored noodles. Noodles were made out of flour, water, salt and ground-up seaweed (dried laver) and were both stimulating to the animal and mechanically stable under water when cut into strips with a cross section of 2 mm×2 mm. The noodles were wound around a spool mounted on the front of the capsule holding the animal (Fig. 1C). The animal was fed the end of the strip before being moved into the imaging region, and it continued eating throughout the imaging procedure.

A sequence of three successive orthogonal images taken during swallowing is shown in Fig. 2. Comparisons of animals eating seaweed strips and seaweed-flavored noodles indicated no differences in interswallow intervals or willingness to feed. MRI data were also obtained from animals consuming thin strips of seaweed, making swallowing movements in response to seaweed extract, swallowing in response to polyethylene tubes with a small piece of seaweed on the end presented simultaneously with seaweed extract and swallowing in response to string wrapped with seaweed. No qualitative differences in swallowing behavior were observed in response to these different stimuli.

High-spatial-resolution MRI measurements

Two animals were anesthetized with an injection of 333 mmol l^{-1} $MgCl_2$, and their buccal masses were imaged at high spatial resolution. One buccal mass was imaged on the Elscint system, and each pixel had a resolution of 0.3 mm×0.3 mm, over 96 s. The detailed parameters for each scan are as follows: sequence type, fast spin echo; TE (time to echo), 120 ms; TR (time to repeat), 900 ms; NEX (number of excitations), 4; acquisition matrix, 256×256; FOV (field of view), 7.7 cm×7.7 cm; slice thickness, 1.0 mm; tip angle, 90 °. A second buccal mass was imaged on a GE Medical Systems 1.5T Signa MRI system using a solenoid transmit/receive coil, and each pixel had a resolution of 0.1 mm×0.1 mm. The detailed parameters for each scan are as follows: sequence type, fast spin echo; TE, 120 ms; TR, 3000 ms; ETL (echo train length), 16; FOV, 5; SW (slice width), 1.5; AM (acquisition matrix), 512×512; NEX, 4. A high-resolution image of the buccal mass is shown in Fig. 3B.

Kinematic measurements from magnetic resonance images

Definition of standard reference length

To normalize lengths among animals so as to combine measurements from odontophores of different sizes, it was necessary to create a reference length. We chose the internal width of the radular stalk in the mid-sagittal plane at its widest point in the anterio-posterior direction with the long axis of the stalk oriented vertically (Fig. 3A,B), because this width can be readily viewed in magnetic resonance (MR) images of high

temporal resolution. To relate this width to the external width of the radular stalk at this point, which can be readily measured externally in intact buccal masses, we computed the ratio of the inner width to the outer width of the radular stalk, as measured in high-resolution mid-sagittal MR images, in a fixed buccal mass (fixed in 10 % v/v formalin in 333 mmol l^{-1} $MgCl_2$, pH 7.5) and in freshly isolated radular stalks. To measure this ratio in the isolated radular stalks and the fixed buccal mass, they were sectioned in the mid-sagittal plane, and the stalk wall thickness was measured (Fig. 3A,B). The ratio was determined to be 0.878±0.017 (mean ± S.D., N=1 from histology, N=2 from freshly dissected buccal masses, N=2 from high-spatial-resolution MR images). All lengths were normalized to units of internal radular stalk width, which we refer to as RSW units.

An outline of the radular stalk was superimposed on each MR image (Fig. 4A). The mid-sagittal shape of the radular stalk outline was obtained by performing a three-dimensional reconstruction of the radular stalk shape from high-resolution MR images (Fig. 3C) and then sectioning it mid-sagittally (Fig. 3D). The resulting stalk outline is scaled from a single frame for each sequence so that it fits onto the stalk in the image, and its scale and shape are then fixed for all remaining frames in that sequence.

Extraction of mid-sagittal kinematic parameters

Six *Aplysia californica* (size range 400–580 g, obtained from Marinus, Long Beach, CA, USA) were utilized for these studies. Animals were kept in a 30 l aquarium filled with artificial sea water (Instant Ocean, Mentor, OH, USA) and kept at a temperature of 16 °C. In the slug holding capsule, in which the behavioral responses were recorded, temperatures ranged from 16 to 22 °C during the course of an experiment. In total, 139 swallows were obtained. Swallows were analyzed to find those that were truly mid-sagittal and had minimal parallax on the basis of the interleaved orthogonal images and the highest image quality throughout

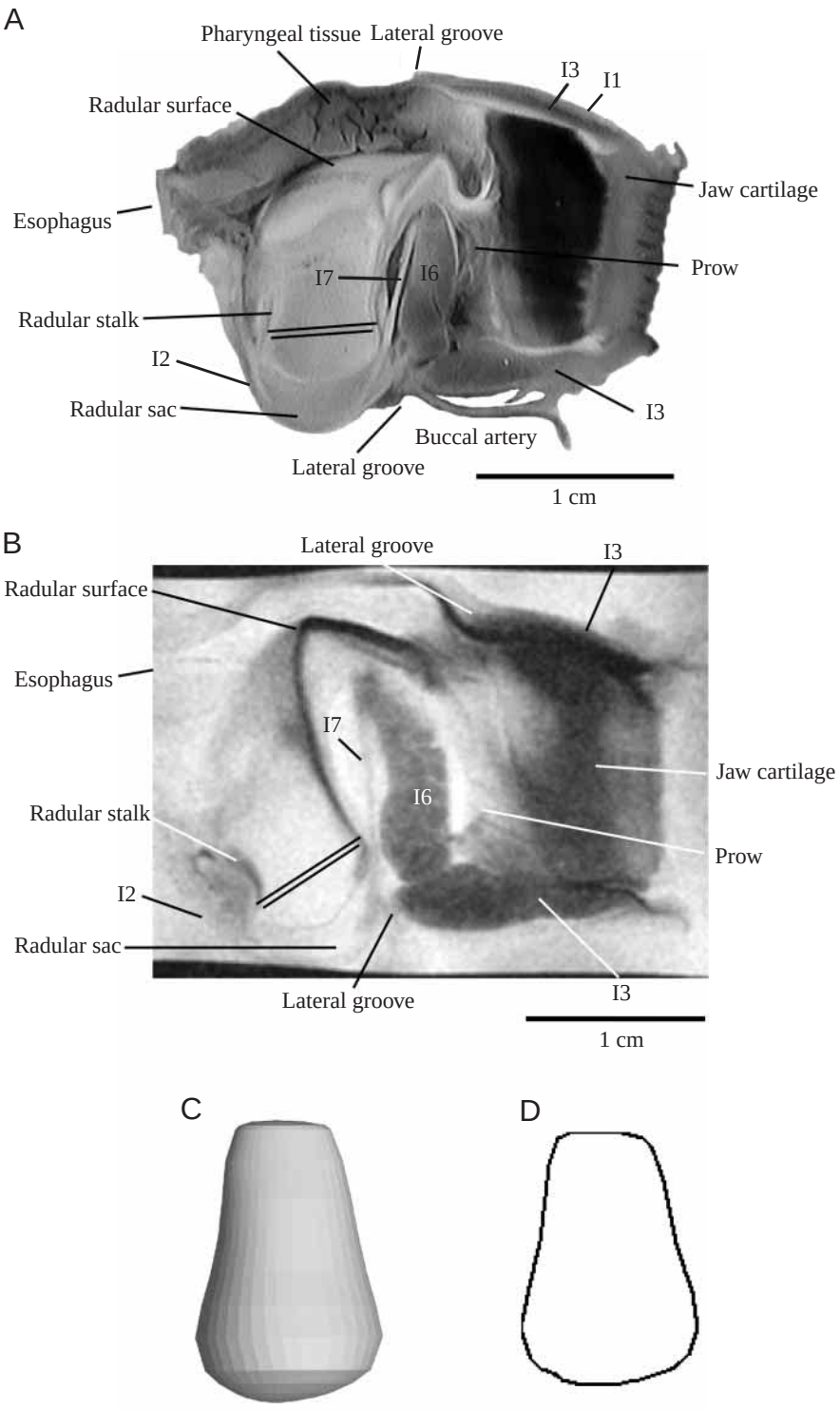

Fig. 3. Mid-sagittal anatomy of buccal mass and radular stalk measurements. Key anatomical features visible in mid-sagittal fixed tissue (A) and in high-spatial-resolution magnetic resonance (MR) images (B) are indicated. The features outlined in the high-temporal-resolution MR images (see Fig. 4) are visible. To create a reference length for measurements that could be reliably measured on the high-temporal-resolution MR images, the length of the inner width of the radular stalk was used. To relate this width to external measurements of radular stalk width, we measured the ratio of the outer to the inner widths in fixed tissue (A), in high-resolution MR images (B) and in freshly dissected tissue (not shown). (C) Radular stalk shape based on a three-dimensional reconstruction of high-resolution MR images. (D) Mid-sagittal view of radular stalk shape based on the three-dimensional reconstruction shown in C.

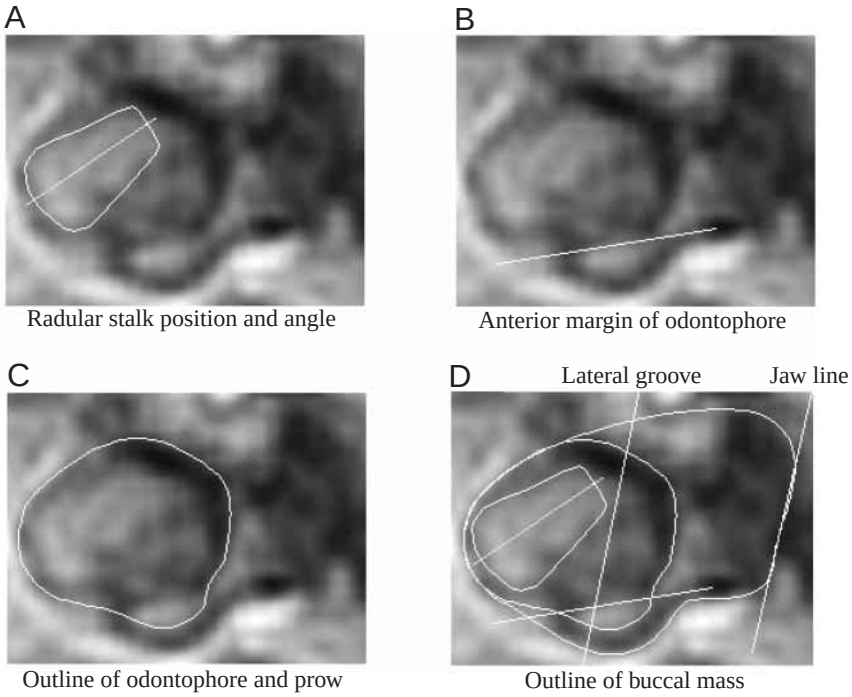

Fig. 4. Measurements on high-temporal-resolution magnetic resonance images. The same image is shown in A–D. (A) Radular stalk outline (see Fig. 3 and text) and a line indicating the axis of the radular stalk. (B) The angle of the anterior margin of the odontophore, determined by the margin of the I6 muscle just posterior to the prow (see Fig. 6 and text). (C) Outline of the odontophore including the prow. (D) Image showing all the measurements shown in A–C and, in addition, an outline of the entire buccal mass (excluding the pharyngeal tissue), the line of the jaws and the line of the lateral groove (the dorsal and ventral border between the I1/I3/jaw musculature and the posterior I2 muscle).

the entire behavior (Fig. 2). On the basis of these criteria, two swallows from each of two different animals were analyzed in detail. Two swallows were in response to seaweed-flavored noodles (swallows 1 and 2) and two swallows were in response to polyethylene tubes presented simultaneously with seaweed extract (swallows 3 and 4). Examination and comparison of these sequences with many other MR sequences indicated that they were typical of the range of swallowing responses observed.

To identify structures of the buccal mass in the high-temporal-resolution MR images, images were compared with histological cross sections (e.g. Fig. 3A) and with high-spatial-resolution MR images (e.g. Fig. 3B). In addition, the entire sequence of high-temporal-resolution MR images for each behavior was displayed as a QuickTime movie (version 4.1, Apple Computer, Inc., Cupertino, CA, USA). Successive images were repeatedly played to enhance and clarify changes that occurred from image to image that were often subtle but were seen clearly in moving rather than in still images.

To measure specific features, each image was imported into Paint Shop Pro (version 7.0, JASC Software, Eden Prairie, MN, USA), and the following kinematic measures were drawn on each image in different layers: (i) jaw line, (ii) radular stalk outline and radular stalk angle, (iii) lateral groove (the borders of the I1/I3/jaw musculature dorsally and ventrally), (iv) odontophore angle (the angle of the anterior edge of the I6 muscle), (v) an outline of the odontophore, excluding the base of the radular stalk if it protruded below the odontophore, and (vi) an outline of the entire buccal mass including the jaw musculature, the odontophore and the radular stalk, but excluding the pharyngeal tissue because it is only partially visible in these images (Fig. 4). Each analyzed MR image was then imported into Animation Shop (version 3.0, JASC Software), and each layer was saved as a separate TIFF image. Measurements of parameters were then performed on these TIFF images using custom-designed programs written in IDL (version 5.4, Research Systems Inc., Boulder, CO, USA; code available from the authors on request). The resulting data was analyzed and displayed using *Mathematica* (version 4.1, Wolfram Corporation, Inc., Champaign, IL, USA).

The feeding cycle was normalized on the basis of definitions of the components of the swallowing cycle from our previous work (Drushel et al., 1997, 1998). Our initial definition of the start of the cycle, which we designated *t1*, was based on the movement from peak protraction to peak retraction, since this was an unequivocal movement that was easy to see in the transilluminated slugs. However, it is clear from our own work and that of others that the feeding cycle is initiated from the onset of protraction (Hurwitz et al., 1996; Hurwitz and Susswein, 1996). As a consequence, we begin the cycle from the onset of protraction, which was designated *t4* in our original definiton of the cycle. Furthermore, in our original study, we designated the inter-swallow interval as *t3*. Examination of successive swallows imaged using magnetic resonance demonstrated that the *t3* interval was extremely variable, whereas the other cycle durations were more consistent. We therefore excluded the *t3* interval from our analysis. The time intervals are therefore defined as follows, using the nomenclature adopted in our original papers for consistency: *t4*, start of anterior buccal mass movement to peak protraction; *t1*, peak protraction to peak retraction; *t2*, peak retraction to the loss of the Γ shape, i.e. the shape in which the base of the elongated radula/odontophore extends ventral to the long axis of the buccal mass (see fig. 3A in Drushel et al., 1997). Cycle times are normalized to the sum of the times *t4+t1+t2*.

Lengths l were normalized to $100(l–l_{min})/(l_{max}–l_{min})$, so that lengths ran from 0 at l_{min} to 100 at l_{max}. After normalization and averaging, data were smoothed using an interpolation function, which fitted cubic polynomials between successive

data points. In addition, functions for the standard deviation of the data were constructed as follows: interpolation functions for each individual normalized data set were subtracted from the interpolation function for the averaged normalized data set, and these differences were summed, squared and divided by the number of samples minus 1 (i.e. by 4–1=3), and then the square root of the function was taken. The normalized, averaged data function is plotted, as well as the normalized, averaged data function with the standard deviation function added to or subtracted from it. This provides an indication of the dispersion around each point in the averaged function. Inferences about significant changes in kinematic variables during the swallowing cycle are drawn only if two points on the averaged curve differ by more than two standard deviations.

Results

Overall kinematics of swallowing

A complete sequence of high-temporal-resolution mid-sagittal MR images during a single swallow is shown in Fig. 5. Each image is shown in three ways: as the original MR image, as the MR image with the kinematic measurements superimposed on it (see Fig. 4) and as the kinematic measurements alone. Several features of the swallowing behavior are clear from the images. The cycle is initiated with an anterior translation and rotation of the odontophore, as seen by the rotation of the odontophore angle and the radular stalk (frames 1–4). The overall shape of the odontophore flattens as it protracts through the I1/I3/jaw musculature, and internal movements of the components of the odontophore are visible (frames 2–5). At peak protraction (frame 9), the most anterior part of the radula/odontophore nearly reaches, but does not pass, the line of the jaws.

After peak protraction, the odontophore rotates and translates posteriorly, and the radular stalk moves in an increasingly posterior direction relative to the base of the odontophore until it protrudes through the ventral surface of the odontophore (frames 10–18; we refer to this as ‘moving out of the odontophore’). The radular stalk then moves very rapidly towards what at rest would be the dorsal surface of the odontophore (frames 19–20; we refer to this as ‘moving into the odontophore’). The movement of the radular stalk into the odontophore corresponds to the loss of the overall Γ shape of the buccal mass (Drushel et al., 1997). A pinching together of the dorsal and ventral surfaces of the buccal mass at the level of the lateral groove is visible at the end of retraction (frames 19–21) as the odontophore ceases to rotate and translate posteriorly and begins to move anteriorly again.

These results are consistent with observations of swallowing-like behaviors in semi-intact and reduced preparations (Drushel et al., 1998) and with the changes in shape described in our studies of juvenile transilluminated animals (Drushel et al., 1997). The temporal and spatial resolution of these images make it possible to describe movements of buccal muscles whose borders are visible in the mid-sagittal image, movements of the odontophore relative to the whole buccal mass and movements within the odontophore itself.

Kinematics of the prow

On the anterior surface of the buccal mass is a small structure that has not been described previously, which we refer to as the prow, since its shape is reminiscent of the prow of a ship (Fig. 6A–C). Anatomical analysis indicated that muscle fibers run along its anterior side (Fig. 6D) and that it is filled with a jelly-like fluid whose consistency is similar to the fluid filling the radular sac. Because it is water-filled, it appears as a bright area on the anterior surface of the odontophore in the MR images (Figs 3B, 4C). The anterior surface of the prow is rounded during protraction and during the initial phases of retraction (Fig. 5, frames 1–10). During protraction, it is pressed up against the ventral I3 musculature (Fig. 5, frames 3–9). As the radular stalk protrudes through the ventral surface of the odontophore, the prow becomes elongated and thinner (Fig. 5, frames 11–19; it is thinnest in frame 19). After a strong retraction, the prow is the first part of the odontophore to extend anterior to the lateral groove and into the region of the I1/I3/jaw musculature (Fig. 5, frames 20–22).

Kinematics of buccal muscles I2 and I3

Because the lateral groove is visible in high-temporal-resolution mid-sagittal MR images, it is possible to determine the cross-sectional length of the I2 muscle (a thin protractor muscle that wraps around the posterior part of the buccal mass) (Hurwitz et al., 1996) and also to measure directly the antero-posterior lengths of the I1/I3/jaw musculature dorsally and ventrally (Fig. 3A,B). Thus, we can measure the kinematics of these muscles of the buccal mass directly during a swallowing cycle. It is possible to visualize directly the I7 muscle in the high-spatial-resolution MR images (Fig. 3B), but it is too small to visualize directly in the high-temporal-resolution MR images (Fig. 4).

I2 kinematics

We measured the length of the I2 muscle from the dorsal lateral groove to the ventral lateral groove around the posterior end of the buccal mass. In the four sequences that we measured, we observed that I2 shortened from the start of anterior buccal mass movement to peak protraction (Fig. 7A–E, *t4* period; Fig. 5, frames 1–9), lengthened from peak protraction to peak retraction (Fig. 7A–E, *t1* period; Fig. 5, frames 9–18) and then shortened from peak retraction to the loss of the Γ shape (Fig. 7A–E, *t2* period; Fig. 5, frames 18–20). There is an inflection point in the length of I2 during the middle of retraction in three of the four swallows (Fig. 7B–E, *t1* period). The inflection in the I2 length corresponds to the images during which the lengthened radula/odontophore rotates and moves posteriorly to the lumen of the jaws (Fig. 5, frames 16–18). Swallow 1, which is the

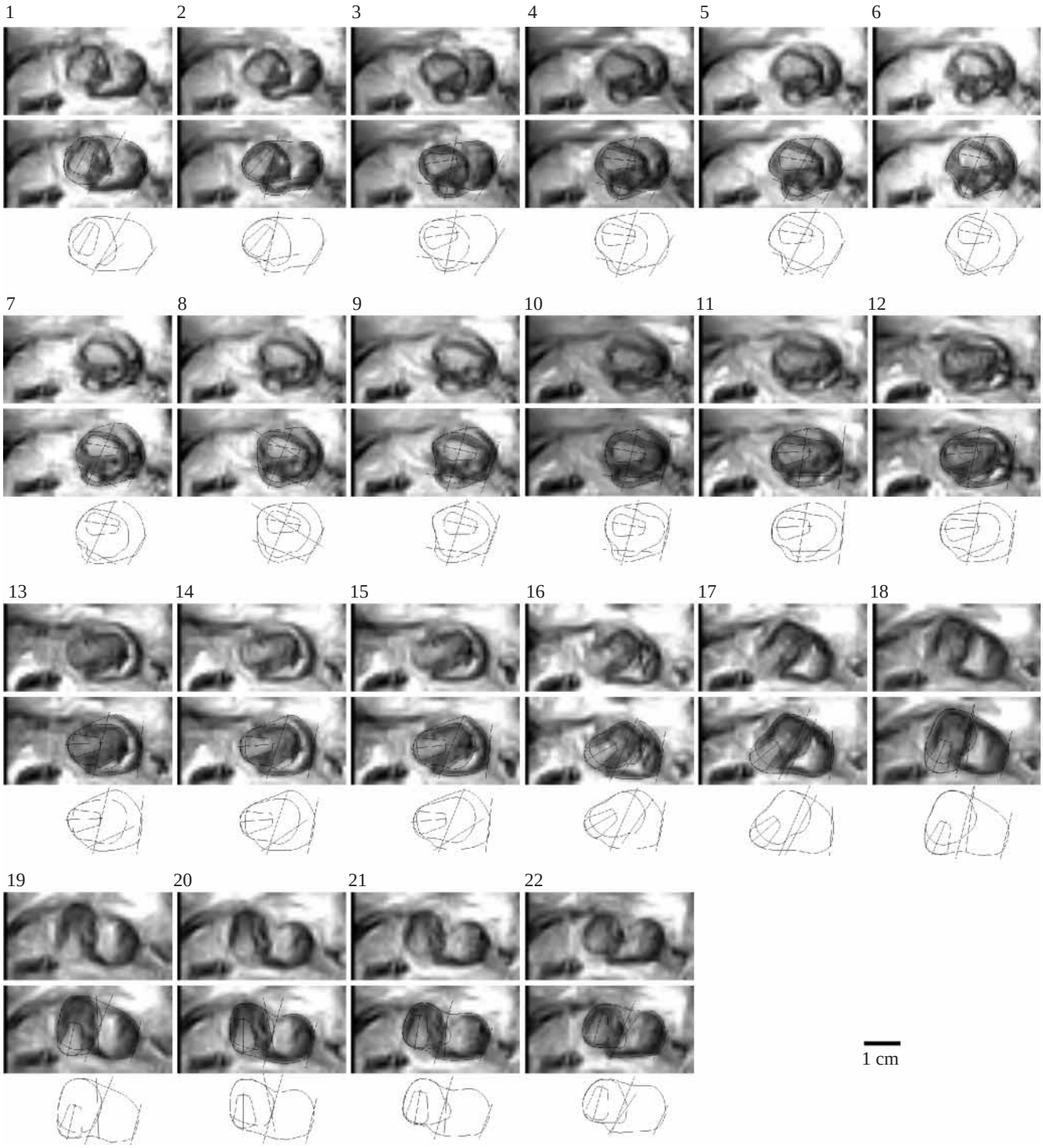

Fig. 5. A sequence (frames 1–22) showing swallowing of a polyethylene tube and its associated kinematic measures. Frames are acquired in 155 ms and are separated by 310 ms. The top row shows the high-temporal-resolution data; the middle row shows these images with the kinematic measures (described in Fig. 4) superimposed and the bottom row shows the kinematic measures alone. This corresponds to swallow 4, data for which are shown in part D of Figs 7–13.

weakest swallow, shows little or no inflection (Fig. 7A, *t1* period). Previous estimates of the changing I2 length based on data from transilluminated juvenile slugs and a kinematic model of the buccal mass show excellent correspondence to the directly measured MRI data, reaching a minimum at the end of protraction and a maximum at the end of retraction (compare Fig. 7E,F) [data in Fig. 7F replotted from Drushel et al. (1998)].

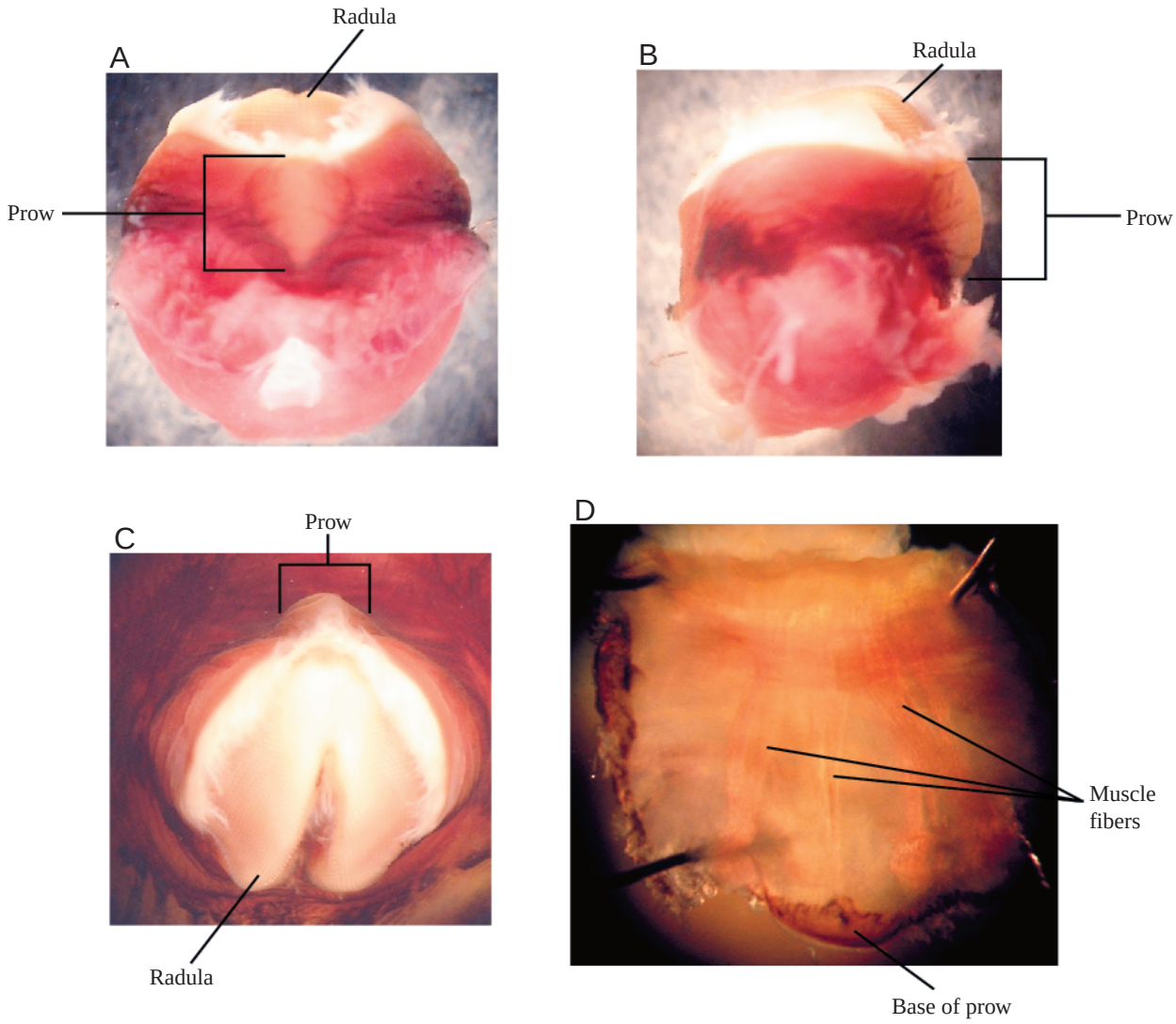

Fig. 6. Anatomy of the prow of the odontophore. (A) External anatomy, anterior view. (B) External anatomy, lateral view. (C) External anatomy, dorsal view. The prow shown in these views was approximately 4 mm in medio-lateral length, 8 mm in dorso-ventral length and 4 mm in antero-posterior length. (D) Internal muscle fibers of the prow. The view is posterior, looking at the inside of the antero-medial surface of the prow.

I3 kinematics

We measured the antero-posterior length of the I3 muscle in the mid-sagittal images. The antero-posterior lengths of the dorsal and ventral parts of the I3 muscle behave differently during the swallowing cycle. The primary changes in antero-posterior length of the ventral I3 are due to the rotation of the odontophore and its effect on the 'hinge', the point of connection between the base of the odontophore (the ventral I4 muscle) and the ventral I3 muscle. As the odontophore rotates towards the jaws during the onset of protraction, the hinge is stretched backwards, causing the ventral surface of the I3 muscle to lengthen (Fig. 8A–E, right panels, *t4* portion of the cycle; Fig. 5, frames 2–8). After the peak of protraction, the odontophore rotates towards the esophagus, the stretch is relieved, and the ventral portion of I3 shortens; it then shortens still further with the loss of the Γ shape after the peak of retraction (Fig. 8B–E, right panels, *t2* portion of the cycle; Fig. 5, frames 11–19; the Γ shape is not large in swallow 1, so additional shortening is not observed in the *t2* portion of the cycle; Fig. 8A, *t2* portion of cycle).

The major changes in antero-posterior length of the dorsal I3 muscle appear to reflect the extent to which the odontophore has inserted itself between the halves of the lumen of the jaw. As the odontophore pushes anteriorly into the jaw musculature, the dorsal I3 shortens (Fig. 8A–E, left panels, during the *t4* portion of the cycle; Fig. 5, frames 2–9). During retraction, as the lengthened odontophore begins to rotate posteriorly and makes contact dorsally with the I3 muscle, the dorsal length of the I3 muscle is at its shortest; it then rapidly increases in length as the odontophore withdraws posteriorly from the jaw lumen (Fig. 8B–E, left panels, during the end of the *t1* portion

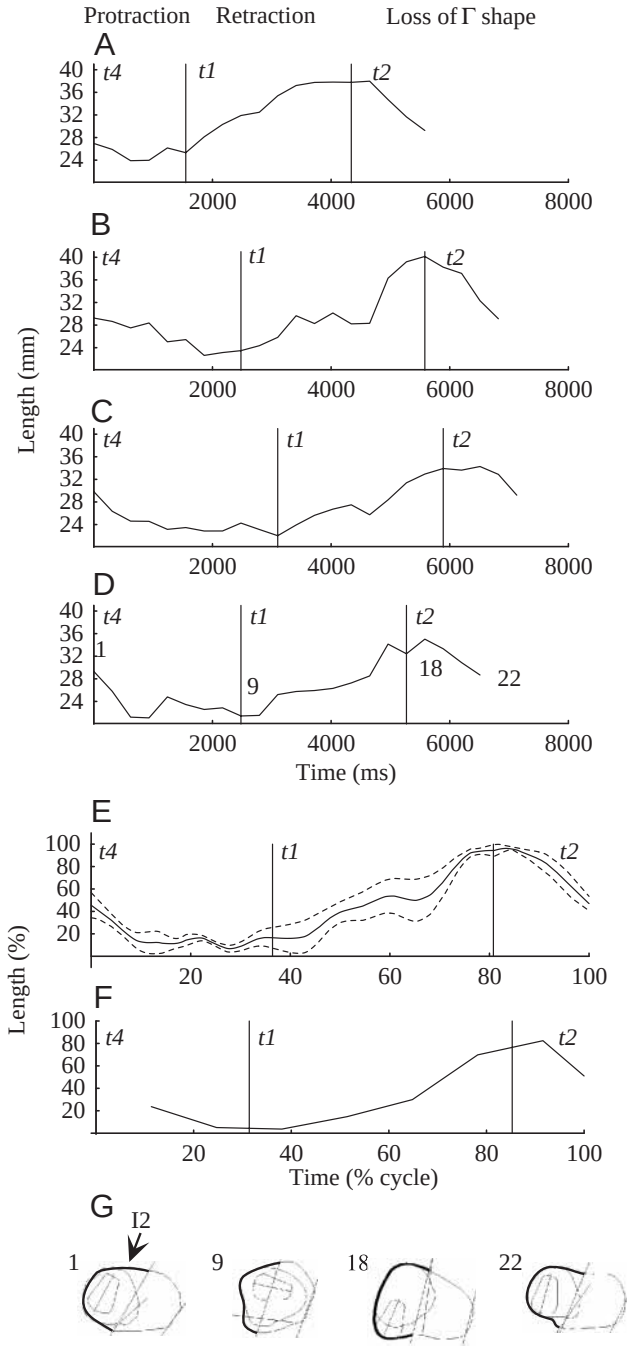

Fig. 7. Kinematics of the I2 muscle during swallowing. Data in A–D are plotted as length (mm) as a function of time (ms). (A) I2 kinematics in the first swallow. The first sequence from the images in set 7725 starts with image 27 and ends with image 44. The onset of the *t4* period is frame 27, the onset of the *t1* period is frame 32 and the onset of the *t2* period is frame 41; each of these period onsets is indicated using a vertical line. For definitions of periods *t1*, *t2* and *t4*, see Materials and methods. (B) I2 kinematics in the second swallow. The second sequence from the images in set 7725 starts with image 45 and ends with image 67. The onset of the *t4* period is frame 45, the onset of the *t1* period is frame 53 and the onset of the *t2* period is frame 63. (C) I2 kinematics in the third swallow. The first sequence from the images in set 7732 starts with image 16 and ends with image 39. The onset of the *t4* period is frame 16, the onset of the *t1* period is frame 26 and the onset of the *t2* period is frame 35. (D) I2 kinematics in the fourth swallow, whose individual images are shown in Fig. 5. The second sequence from the images in set 7732 starts with image 39 and ends with image 60. The onset of the *t4* period is frame 39, the onset of the *t1* period is frame 47 and the onset of the *t2* period is frame 56. (E) Normalized, averaged and smoothed I2 kinematics during swallowing cycle. Data are shown as the mean ± 1 S.D. (F) Normalized and averaged data from a transilluminated slug (replotted from Drushel et al., 1998) (the cycle starts at *t4*, and cycle length is renormalized to be the sum of the *t4*, *t1* and *t2* periods, excluding the *t3* period). (G) Schematic diagrams indicating the length of I2 plotted in D for frames 1, 9, 18 and 22. I2 is highlighted with a black line. Compare original frames in Fig. 5.

of the cycle; Fig. 5, frames 15–17; this is not seen in Fig. 8A, which shows a weaker protraction and retraction cycle).

Consistent changes are observed in the dorso-ventral length of the I3 muscle at the lateral groove during the swallowing cycle. During the protraction phase, as the odontophore rotates towards the jaws, the I3 muscle at the lateral groove expands (Fig. 9A–E, left panels, *t4* portion of the cycle; Fig. 5, compare frames 1 and 9). During retraction, the length of I3 at the lateral groove decreases; the length reaches a minimum during the loss of the Γ shape, at which time a 'pinching in' of the buccal mass at the lateral groove is sometimes visible (e.g. Fig. 5, frames 19–21; Fig. 9A–E, left panels, *t2* portion of the cycle).

The change in the dorso-ventral length of the I3 muscle at the jaws during the swallowing cycle is more variable than that at the lateral groove. In general, the width of the I3 at the jaws increases later than does the width of the I3 at the lateral groove [Fig. 9E, compare peak in left panel (lateral groove I3 width) during *t4* with peak in right panel (jaw I3 width) during *t1*]. Moreover, the minimum width of the I3 at the jaws occurs after the minimum width in the I3 at the lateral groove (Fig. 9E, *t2* period; compare left and right panels). In some swallows, the jaws show relatively little expansion during the entire cycle (Fig. 9C, right panel), whereas in others, significant expansion is observed (e.g. Fig. 9B,D, right panels).

Odontophore kinematics

We measured bulk movement of the entire buccal mass, movement of the odontophore within the buccal mass, deformations of the odontophore and motions of the radular stalk within the odontophore.

Bulk movement of the entire buccal mass

In previous studies, we observed that the line connecting the jaws and the esophagus could serve as a fixed reference frame for overall movements of the buccal mass (Drushel et al., 1997). In the current study, we observed that the posterior part of the buccal mass was free to move relative to the jaws. We therefore used the line of the jaws as an intrinsic reference frame since it moves rigidly as part of the anterior jaw cartilage. We observed that the motions of the jaw line were quite variable (Fig. 10). The angle of the jaw could change

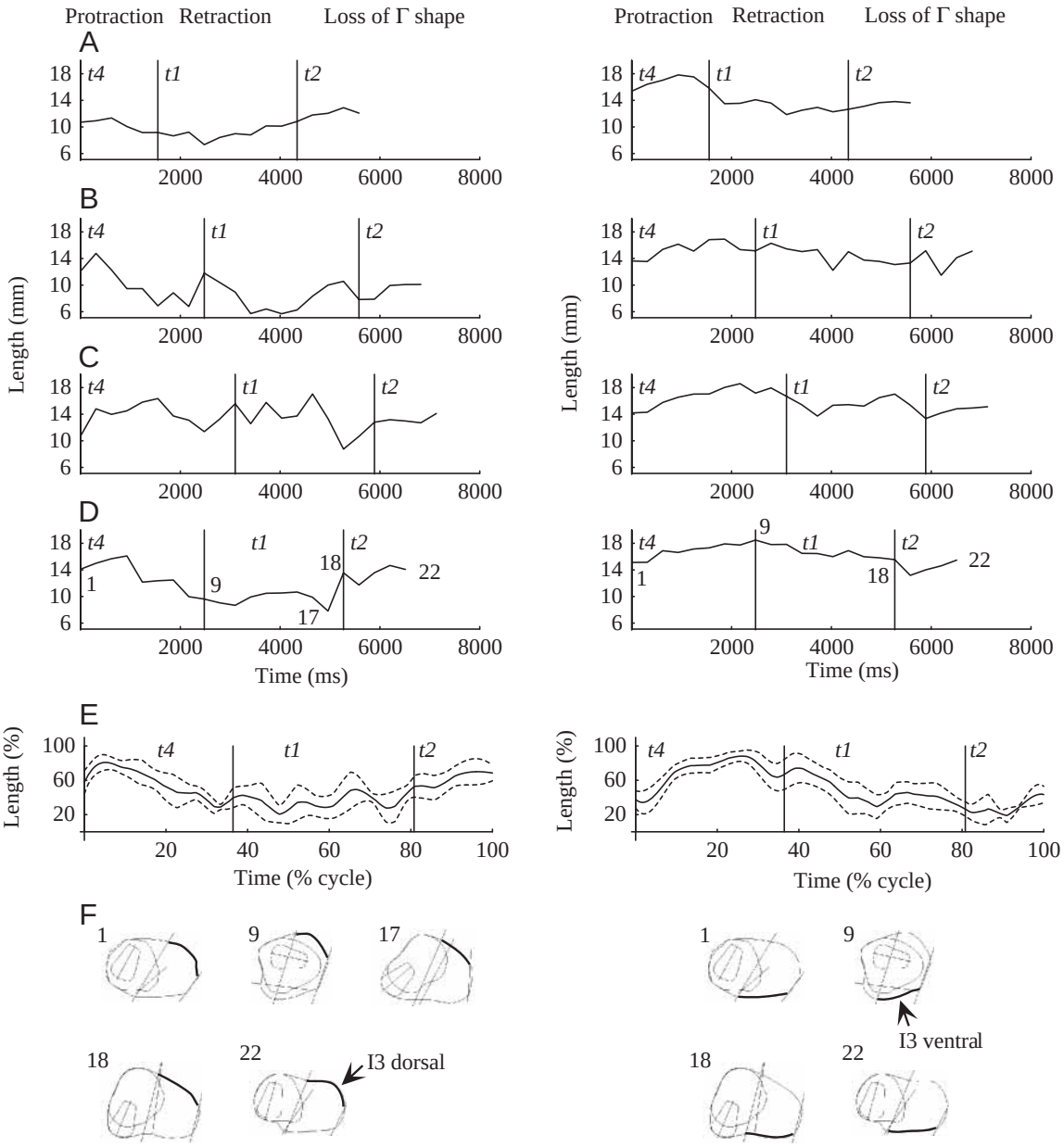

Fig. 8. Kinematics of the antero-posterior length of the I3 muscle during swallowing. (A–D) Data plotted as length (mm) as a function of time (ms). Left panels show the antero-posterior length of the I3 muscle on the dorsal surface. Right panels show the antero-posterior length of the I3 muscle on the ventral surface. (A) I3 kinematics in the first swallow. (B) I3 kinematics in the second swallow. (C) I3 kinematics in the third swallow. (D) I3 kinematics in the fourth swallow. (E) Normalized, averaged and smoothed anterio-posterior lengths of I3 during the swallowing cycle. Data are shown as mean ± 1 S.D. (F) Schematic diagrams indicating the antero-posterior length of I3 on the dorsal surface for frames 1, 9, 17, 18 and 22, highlighted with a black line. The antero-posterior lengths of I3 on the ventral surface for frames 1, 9, 18 and 22 are shown on the right, highlighted with a black line. Compare original frames in Fig. 5. For definitions of periods *t1*, *t2* and *t4*, see Materials and methods.

during protraction or during retraction and could increase or decrease. In one sequence, the difference between the minimum and maximum angle was approximately 10° (Fig. 10A); in the other three sequences, the difference ranged from approximately 25 to 30° (Fig. 10B–D). To correct for these bulk rotations, all rotational and translational movements were referenced to the jaw line in each sequence. Since we orient the jaws to the right and the esophagus to the left, and the dorsal surface of the buccal mass upwards and the ventral surface downwards (see Fig. 2, sagittal section), clockwise angles that move the odontophore towards the jaw line are reported as positive, and translational movements of the odontophore from the esophagus towards the jaw line are reported as positive, in units of radula stalk width (RSW).

Movement of the odontophore within the buccal mass

At the onset of forward movement of the buccal mass, the anterior border of the odontophore (i.e. the anterior border of

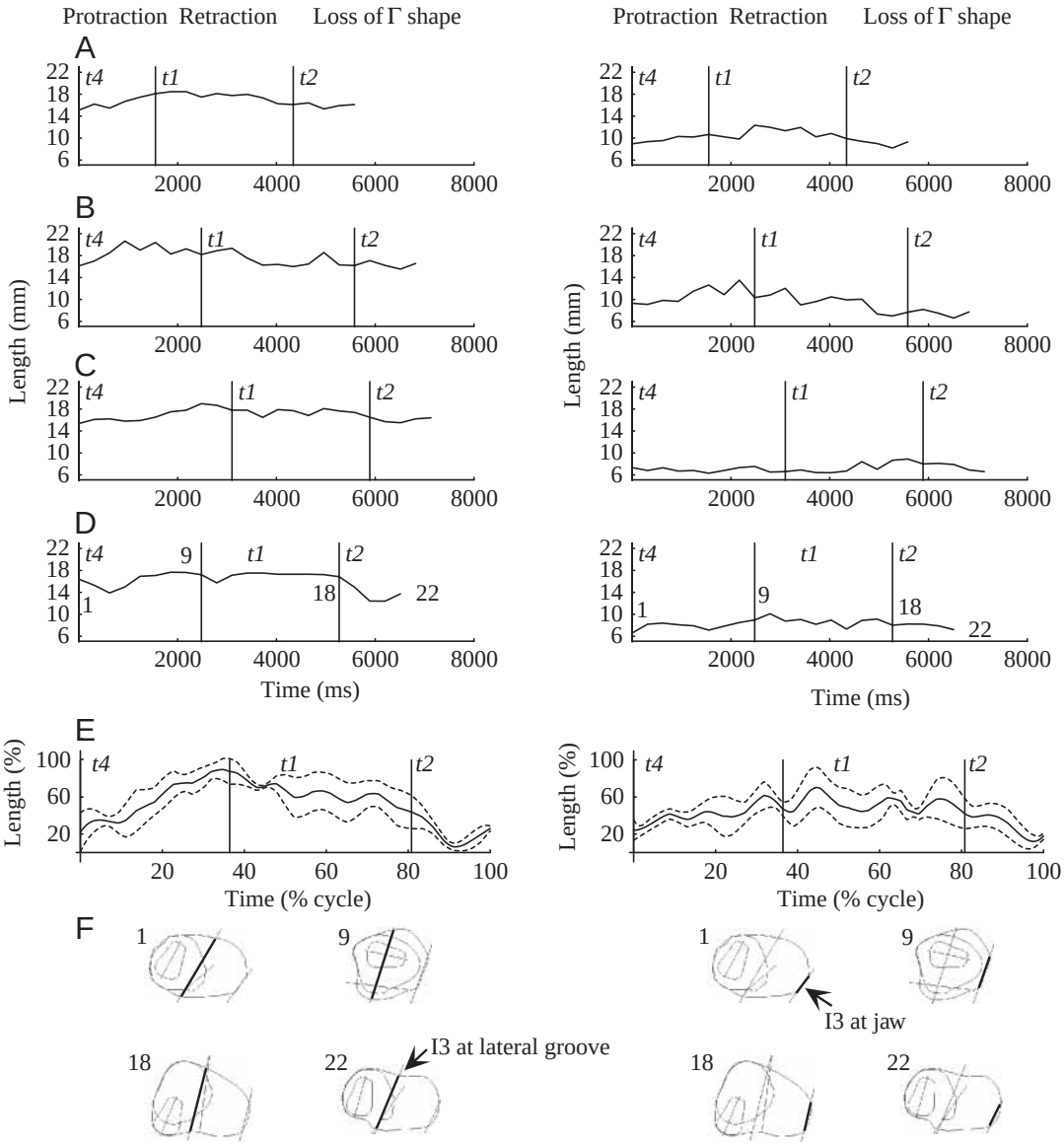

Fig. 9. Kinematics of the dorso-ventral length of the I3 muscle during swallowing. (A–D) Data from each of the four individual swallowing sequences plotted as length (mm) as a function of time (ms). The left panels show the dorso-ventral length of the I3 muscle at the lateral groove. The right panels show the dorso-ventral length of the I3 muscle at the line of the jaws. (E) Normalized, averaged and smoothed dorso-ventral lengths of I3 during the swallowing cycle. Data are shown as mean ± 1 S.D. (F) Schematic diagrams indicating the dorso-ventral length of I3 at the lateral groove for frames 1, 9, 18 and 22, highlighted with a black line. The dorso-ventral lengths of I3 at the jaws for frames 1, 9, 18 and 22 are shown on the right, highlighted with a black line. Compare original frames in Fig. 5. For definitions of periods *t1*, *t2* and *t4*, see Materials and methods.

the I6 muscle) rotates towards the jaws (Fig. 11, left panels; Fig. 5, frames 1–8). Peak rotation towards the jaws ends before the peak of protraction in swallowing (during the *t4* period before the *t1* border; Fig. 11, left traces; note especially the average trace, Fig. 11E, left). The odontophore rotates posteriorly relative to the line of the jaws from before the end of protraction until after the end of retraction (i.e. into the *t2* period; Fig. 11, left panels; Fig. 5, frames 8–20). During the retraction phase, there is an abrupt decrease in angle at the time that the odontophore withdraws posteriorly from the jaws (Fig. 11, left panels, during the *t1* period; Fig. 5, frames 15–18).

In contrast, the translation of the most anterior tip of the odontophore towards the jaws continues past the peak of protraction (i.e. into the *t1* period, after retraction of the posterior end of the buccal mass has begun; Fig. 11, right panels; Fig. 5, frame 10). The anterior tip of the odontophore then moves posteriorly relative to the jaw line throughout retraction and even past peak retraction (i.e. into the *t2* period when the Γ shape is lost; Fig. 11, right traces; Fig. 5, frames 11–20). Note that during retraction, at the same time that there is a rapid decrease in angle, there is also a rapid posterior motion, which corresponds to the time at which the

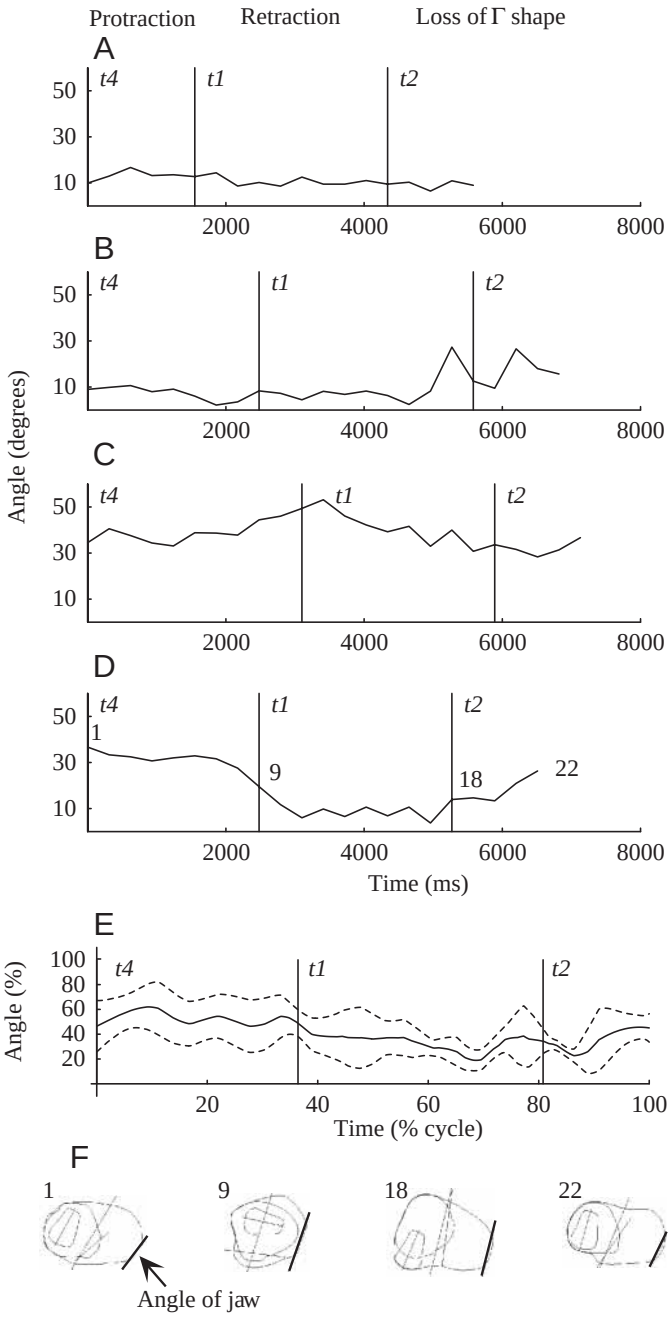

Fig. 10. Overall movement of the buccal mass based on the changing angle of the jaw line relative to the fixed tank holding the animal. (A–D) Data from each of the four individual swallow sequences plotted as angle (degrees) as a function of time (ms). (E) Normalized, averaged and smoothed jaw line angle during the swallowing cycle. Data are shown as mean ± 1 S.D. Note that all four swallows show different patterns of change in the angle of the jaws. (F) A black line is used to highlight the jaw angle for frames 1, 9, 18 and 22. Compare original frames in Fig. 5. For definitions of periods *t1*, *t2* and *t4*, see Materials and methods.

odontophore withdraws from the jaws (Fig. 11, right panels, during the *t1* period; Fig. 5, frames 15–18). The timing of the odontophore movements does not correspond exactly to the borders of the *t4*, *t1* and *t2* periods because these periods are defined by the timing of movements of the posterior border of the buccal mass, and the timing of the internal movements and deformations of the odontophore (see below) does not exactly correspond to these movements.

Deformations of the odontophore

We examined the changes in the dorso-ventral and antero-posterior length of the odontophore during a swallowing cycle. To provide a reference frame for these deformations, we rotated the outline of the odontophore so that the anterior border of I6 was vertical, and then determined the maximum dorso-ventral and antero-posterior lengths of the odontophore's outline in this position. The antero-posterior length extended only to the anterior border of I6 and excluded the changing thickness of the prow in order to determine the changing dimensions of the solid muscle and cartilage of the odontophore. The antero-posterior length of the odontophore increased during protraction, as did the dorso-ventral length, but to a lesser extent (Fig. 12, near the end of the *t4* period; compare left and right panels). The dorso-ventral length increased and remained higher during retraction at the same time that the antero-posterior length decreased (Fig. 12, *t1* period; compare left and right panels). The dorso-ventral lengthening of the odontophore at the beginning of the retraction period corresponds to, and accounts for, the positive translation of the anterior end of the odontophore after the onset of the retraction of the posterior end of the buccal mass, which defines the onset of the *t1* period (Fig. 11E, right side, *t1* period). During the loss of the Γ shape, there were decreases in both the antero-posterior and dorso-ventral lengths (Fig. 12, *t2* period). The length changes are not mirror images of one another, especially during the *t2* period, suggesting that some of the changes in these specific dimensions may be compensated for by changes in the medio-lateral width, which is not directly measurable in the mid-sagittal MR images.

Movement of the radular stalk within the odontophore

Movements internal to the odontophore can be examined by measuring the rotations and translations of the radular stalk within the frame of reference of the odontophore. We measured the rotations of the radular stalk relative to the anterior border of the I6, and the translations of the base of the radular stalk relative to the base of the odontophore. At the onset of protraction, the radular stalk moves into the odontophore (Fig. 13, right panels, period *t4*; Fig. 5, frames 1–6) and initially rotates posteriorly relative to the anterior margin of the odontophore (Fig. 13, left panels, period *t4*; Fig. 5, frames 1–2). During the middle of the protraction phase, however, the radular stalk rotates slightly anteriorly and then again rotates posteriorly relative to the anterior margin of the odontophore (Fig. 13, left panels, middle of period *t4*; Fig. 5, frames 3–4 *versus* frames 5–6). During the retraction phase, the radular stalk moves out of the odontophore (Fig. 13, right panels, *t1* period; Fig. 5, frames 10–18) and rotates towards the anterior margin of the odontophore (Fig. 13, left

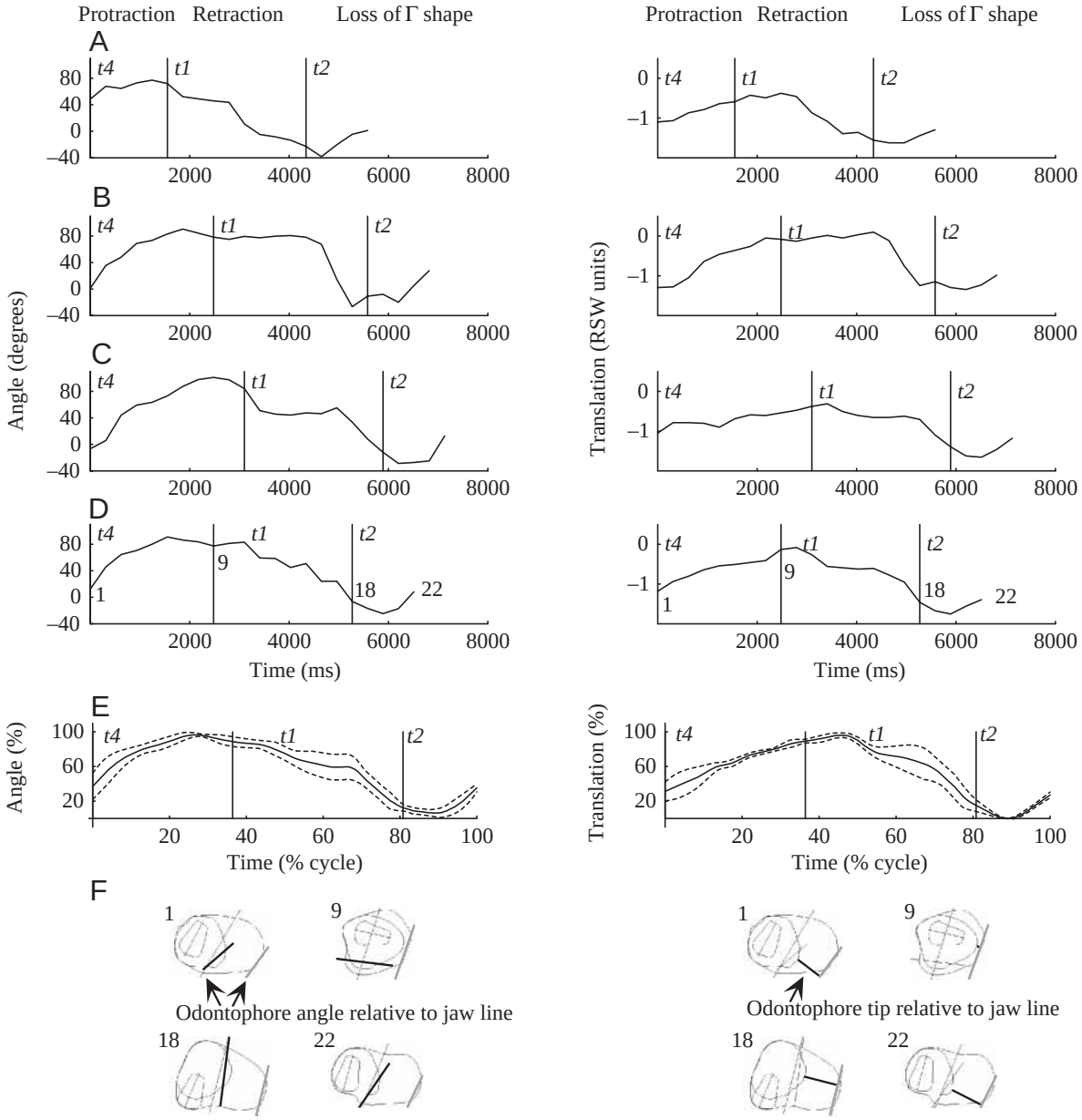

Fig. 11. Movements of the odontophore relative to the buccal mass. The left panels show rotation of the anterior border of I6 relative to the jaw line. The right panels show translation of the anterior tip of the odontophore relative to the jaw line, with the jaw line rotated to be vertical. (A–D) The rotation (left panels, angle as a function of time) and translation [right panels, distance, in units of internal radular stalk width (RSW units) as a function of time] during each of the four individual swallowing sequences. (E) Normalized, averaged and smoothed rotations (left) and translations (right). Data are shown as the mean ± 1 S.D. (F) Schematic diagrams indicating the rotation of the odontophore for frames 1, 9, 18 and 22. The anterior margin of the odontophore is highlighted with a black line, and the jaw line (relative to which the angle is measured) is highlighted with a gray line. The translation of the odontophore for frames 1, 9, 18 and 22 is shown on the right. A gray line highlights the jaws, and a black line indicates the distance from the anteriormost point of the odontophore to the jaw line. Compare original frames in Fig. 5. For definitions of periods *t1*, *t2* and *t4*, see Materials and methods.

panels, *t1* period; Fig. 5, frames 10–15). The radular stalk begins to move back into the odontophore before the end of retraction, whereas the translation and rotation of the odontophore do not change direction until after the end of retraction (compare Fig. 13, right panels, *t1* period, and Fig. 11, left and right panels, *t1* period). As the buccal mass loses its Γ shape, the radular stalk moves back into the odontophore (Fig. 13, right panels, *t2* period; Fig. 5, frames 18–22) and rotates sharply posteriorly relative to the anterior margin of the odontophore (Fig. 13, left panels, *t2* period; Fig. 5, frames 18–22).

Discussion

Using magnetic resonance imaging, we have obtained views

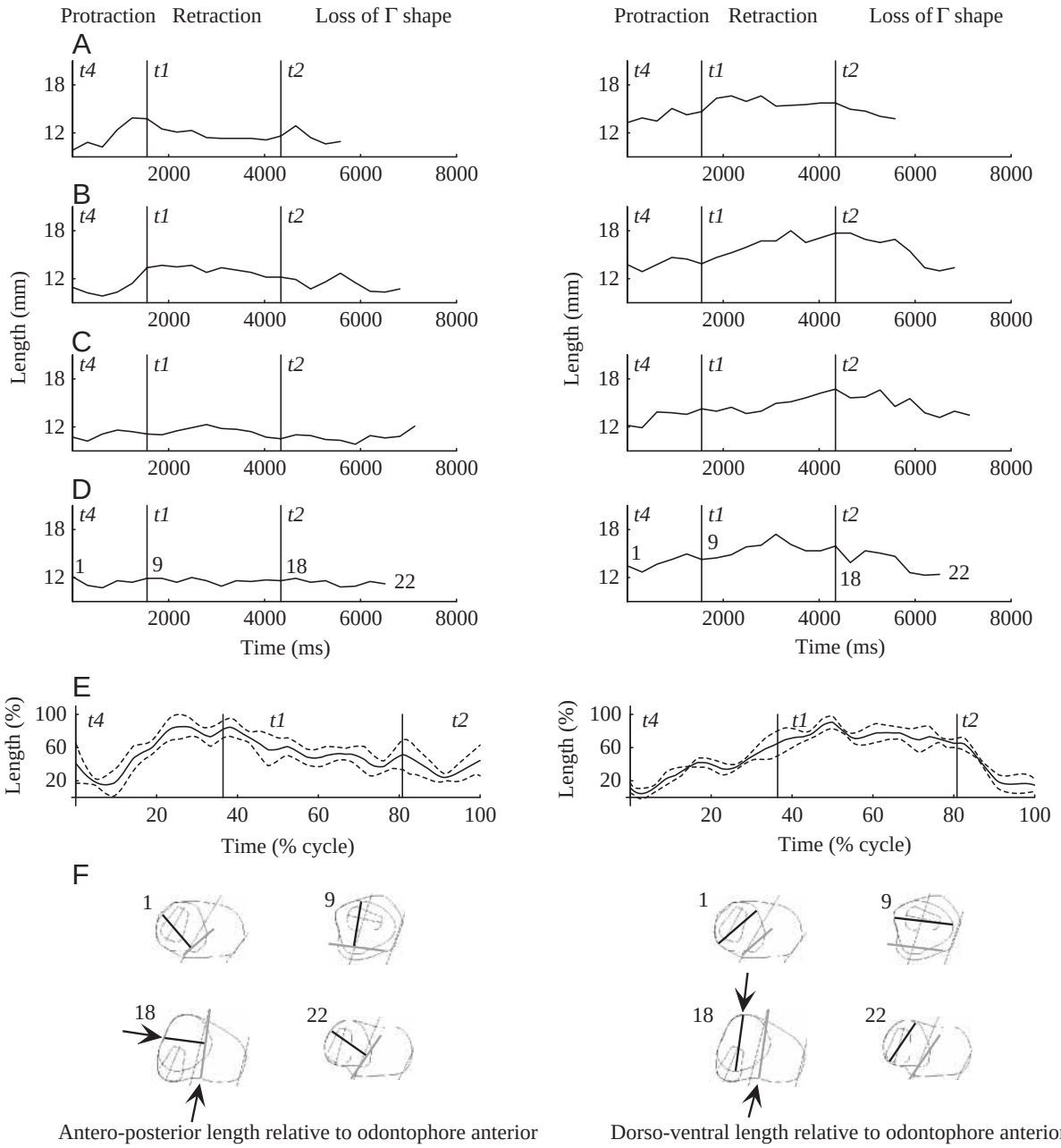

Fig. 12. Deformations of the odontophore during swallowing. To provide an internal reference frame for the odontophore, all measurements were made after the anterior border of I6 had been rotated so that it was vertical. All lengths in A–D are mm plotted as a function of time (ms). The left panels show the changes in the antero-posterior length; the right panels show the changes in the dorso-ventral length. (A–D) Data from each of the four individual swallowing sequences; (E) these data normalized, averaged and smoothed ± 1 S.D. (F) Schematic diagrams indicating the antero-posterior odontophore length for frames 1, 9, 18 and 22. The anterior margin of the odontophore is highlighted with a gray line, and a parallel line drawn at the maximum antero-posterior length is highlighted with a black line. The dorso-ventral lengths of the odontophore for frames 1, 9, 18 and 22 are shown on the right. A gray line highlights the anterior margin of the odontophore, and a black line indicates the maximum length in the dorso-ventral direction perpendicular to this reference line. Compare original frames in Fig. 5. For definitions of periods *t1*, *t2* and *t4*, see Materials and methods.

of the buccal mass of intact *Aplysia californica* during swallowing responses. The images are of sufficient temporal and spatial resolution to allow a characterization of the kinematics of buccal muscles and of the radula/odontophore in the mid-sagittal plane. To our knowledge, this is the first description of the internal kinematics of molluscan feeding in intact, behaving animals. We will briefly discuss the limitations of the measurements and then describe a series of hypotheses that they suggest for the roles of the *in vivo* components of the buccal mass.

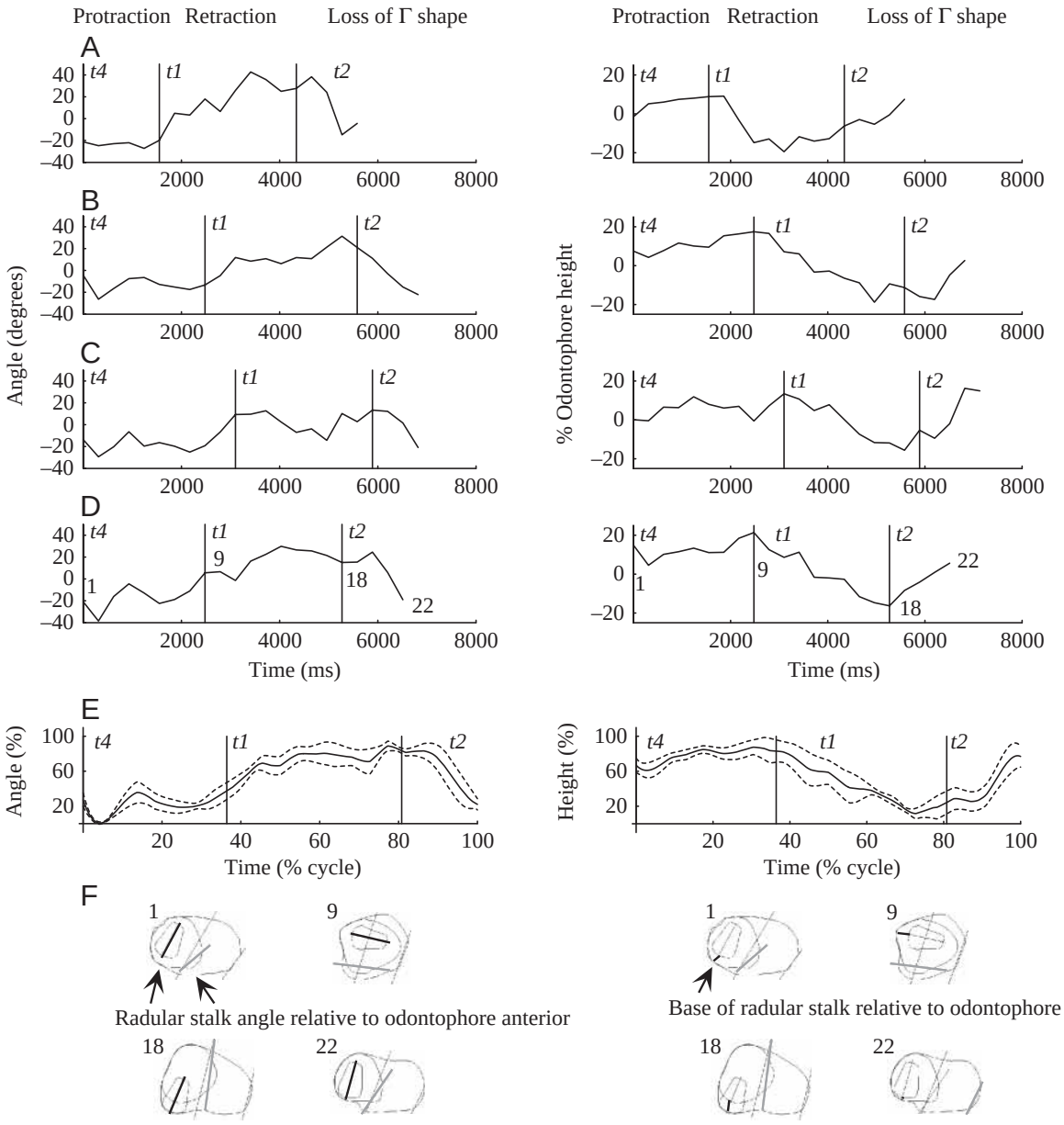

Fig. 13. Movements internal to the odontophore during swallowing. Measurements were made of the rotation of the radular stalk relative to the anterior border of muscle I6 (left panels) and the translation of the base of the radular stalk as a percentage of the dorso-ventral height of the odontophore (right panels). (A–D) Data from individual swallowing sequences. (E) These data normalized, averaged and smoothed ± 1 S.D. Angle (degrees) is plotted as a function of time (ms) in the left panels. Percentage of the odontophore height is plotted as a function of time (ms) in the right panels. (F) Schematic diagrams indicating the rotation of the radular stalk within the odontophore for frames 1, 9, 18 and 22. The anterior margin of the odontophore is highlighted with a gray line, and the line of the radular stalk is highlighted with a black line; the angle is measured relative to the gray line. The translation of the radular stalk for frames 1, 9, 18 and 22 is shown on the right. A gray line highlights the anterior margin of the odontophore, and a black line parallel to this line indicates the distance from the base of the radula to the base of the odontophore. Compare original frames in Fig. 5. For definitions of periods *t1*, *t2* and *t4*, see Materials and methods.

Limitations of MRI measurements

There are several limitations of the magnetic resonance images. The spatial resolution of the images is 1 mm×1 mm, which is small enough to resolve the borders of large structures, but insufficient to directly resolve small muscles such as the I7 muscle (which can be resolved in higher-spatial-resolution MR images; Fig. 3B). Studies of a cylindrical phantom indicated that distortion due to susceptibility artifacts was limited to 1.5 mm, which is also adequate for the accuracy of the reported measurements. Another concern is the possibility of blurring, which could occur if the structure moved from one pixel to another during image acquisition. The overall frequency of the mid-sagittal images (approximately 3 Hz) was low enough that rapid movements of the

odontophore could cause blurring. The actual images are acquired in 155 ms, however, and careful examination of the higher-temporal-resolution movies of the transilluminated slug (Drushel et al., 1997) indicated that even the fastest overall movements of the odontophore, such as its very rapid initial retraction, would not be rapid enough to induce significant blurring.

Another potential limitation could be a movement of the animal that caused the main image to be para-sagittal or to be rotated relative to the mid-sagittal plane of the buccal mass. Careful analysis of the coronal and axial images just preceding and just following the sagittal images allowed us to select sequences in which this possibility was minimized (Fig. 2). Finally, an inherent limitation of the images analyzed in this paper is that they are confined to a single plane, whereas the buccal mass is a three-dimensional structure. This limitation could be overcome either by improvements in MR imaging technology allowing a high-quality full three-dimensional dataset to be acquired at the necessary temporal resolution or by developing three-dimensional kinematic models of the buccal mass that allow the third dimension to be systematically inferred from the mid-sagittal images.

Functional role of the prow of the odontophore

The fluid-filled projection at the anterior border of the odontophore (Fig. 6), which we have called the prow, is likely to play a significant functional role in the protraction and anterior rotation of the odontophore. Since the prow is the first part of the odontophore to extend into the lumen of the jaws, it may act as a wedge to separate the apposed halves of the I3 musculature as the odontophore begins to protract through the lumen of the jaws. Furthermore, the observation that the prow is pressed against the ventral surface of the I3 muscle as protraction proceeds suggests that the effective center of rotation of the odontophore relative to the buccal mass may shift from the odontophore's ventral connection with the I3 muscle (the 'hinge') to the prow during protraction.

Functional implications of the kinematics of I2

In this paper, we provide a first description of the *in vivo* kinematics of the I2 muscle during swallowing based upon internal anatomical borders that define its mid-sagittal extent. Our data are consistent with estimates obtained from juvenile transilluminated slugs (Drushel et al., 1997). It is also possible to analyze these data with respect to values obtained from *in vitro* studies of the length/tension and force/velocity properties of I2 (Yu et al., 1999). Assuming that the length of I2 at the end of the *t2* period is close to the resting length of the I2 muscle, which we showed was equal to $0.86l_{mto}$ (where l_{mto} is defined as the optimal muscle and tendon length of I2), the peak length of I2 at the end of retraction (the end of the *t1* period) is $1.09\pm0.08l_{mto}$ (mean ± S.D., N=4), and the minimum length of I2 at the peak of protraction (the end of the *t4* period) is $0.66\pm0.03l_{mto}$ (mean ± S.D., N=4). Thus, I2 is close to the peak of its length/tension curve at the onset of protraction, providing it with the ability to protract the odontophore strongly. In contrast, it is likely that I2 can generate no more than approximately 40 % of its maximum force near the peak of protraction because of its shortening (see fig. 2C in Yu et al., 1999).

By smoothly interpolating between the length data points and integrating the resulting interpolated function, it is possible to estimate the velocity of the I2 muscle during swallowing (data not shown). In general, the maximum velocity of lengthening of I2 is observed near the end of the retraction phase (*t1* period) as the radular stalk moves out of the odontophore and the odontophore withdraws from the lumen of the jaws ($0.52\pm0.24l_{mto}\,s^{-1}$, mean ± S.D., N=4), suggesting that the maximum force in I2 could be increased by as much as 60 % (see fig. 2D in Yu et al., 1999), which could serve to brake this rapid movement. The maximum velocity of shortening is seen early in the shortening phase of protraction and during the loss of the Γ shape ($0.45\pm0.06l_{mto}\,s^{-1}$, mean ± S.D., N=4), suggesting that the force in I2 could be decreased by as much as 80 % during this rapid contraction.

Functional implications of the kinematics of I3

Although the mid-sagittal view does not provide direct information about the movements of the I1/I3/jaw musculature in the third dimension, several inferences can be drawn from the kinematics reported in this paper: the movement of the 'hinge' point, the muscular hydrostatic properties of the structure, the 'pinch' at the lateral groove and the relative expansion of the lumen of the jaw musculature at the lateral groove *versus* the line of the jaws.

The ventral fibers of the base of the odontophore (the I4 muscles) interdigitate with the fibers of the underlying ventral I3 muscle at the lateral groove. We have used the term 'hinge' to describe this interdigitation since it is clear in isolated semi-intact preparations that the odontophore rotates around this point. The kinematics of the antero-posterior length of the I3 demonstrates that the 'hinge' is not a rigidly fixed point but is stretched as the odontophore rotates anteriorly or posteriorly. Over the course of a swallowing cycle, the antero-posterior length of I3 on the ventral surface of the buccal mass undergoes a 44±5 % expansion (mean ± S.D., N=4) from its minimum length at the maximum posterior rotation of the odontophore (Fig. 8, right panels, *t2* period, and Fig. 11, left panels, *t2* period) to its maximum length at maximum anterior rotation of the odontophore (Fig. 8, right panels, *t4* period, and Fig. 11, left panels, *t4* period).

Changes in the antero-posterior length of the I3 muscle on the dorsal surface of the buccal mass may reflect the muscular hydrostatic properties of the jaw musculature. The length of I3 decreased relative to its maximum length (by 28±17 %, mean ± S.D., N=4) when the tip of the odontophore was furthest anterior, i.e. most fully protracted into the lumen of the jaws, compared with when the tip of the odontophore was furthest posterior relative to the line of the jaws, i.e. most fully retracted out of the lumen of the jaws. When the odontophore is most fully protracted into the lumen of the jaws, it should maximally stretch the lumen of the jaws in the medio-lateral dimension.

To maintain the volume of the structure, the musculature should compress it in its antero-posterior dimension. Conversely, when the odontophore is most fully retracted from the lumen of the jaws, the jaws should be minimally stretched in the medio-lateral dimension, leading to expansion in the antero-posterior dimension to maintain the same volume.

As the buccal mass loses its Γ shape, the dorso-ventral length of the I3 muscle at the lateral groove decreases (Fig. 9, middle of *t2* period, left panels). This corresponds to a pinching together that is visible at the lateral groove (Fig. 5, frames 19–21). This pinch may serve to aid the process of retraction by pushing the radula/odontophore further backwards into the esophagus.

The different anatomical characteristics of the I1/I3/jaw musculature may be reflected in the relative expansions that occur in the structure dorso-ventrally at the lateral groove *versus* at the line of the jaws. Underlying the anterior I3 musculature are plates of jaw cartilage, joined dorsally and ventrally, which are stiff and thus presumably strongly resistant to expansion when stretched very slightly beyond their rest length. At rest, the posterior extent of the cartilaginous plates is only half the antero-posterior length of the jaw musculature (Fig. 3A; note the position of the posterior end of the cartilage in comparison with the location of the lateral groove, which marks the posterior border of the I3 musculature). The remaining section of the I1/I3/jaw musculature complex is composed solely of muscle and of pharyngeal tissue, which are presumably much more distensible.

The ratios of the dorso-ventral length of the I3 muscles at the lateral groove to the dorso-ventral length at the jaw when neither is significantly stretched (i.e. just before the onset of protraction) differ by a factor of 2.05±0.22 (mean ± S.D., N=4). From the material properties of the anterior *versus* posterior sections of the I1/I3/jaw musculature, one might predict that the jaw cartilage would resist expansion more than the musculature at the posterior end of muscle I3. However, since the dorso-ventral length of the jaw cartilages is much smaller to begin with, it is possible that the jaws must undergo a proportionally larger expansion. It is clear from the data that, at their maximum expansion, the dorso-lateral length of the I3 and its underlying cartilage at the jaw line are never as large as the dorso-lateral length of the I3 at the lateral groove, even at its minimum value (Fig. 9A–D; compare left and right panels). However, the relative expansion of the dorso-lateral length at the jaw line is greater than the expansion at the lateral groove: the ratio of the percentage expansion at the jaws to the percentage expansion at the lateral groove is 2.1±0.82 (mean ± S.D., N=4). It is interesting to note that there are folds in the anterior cartilage of the jaws that straighten out as the jaw is stretched, and this may allow the jaw to expand significantly before its resistance to tensile stress sharply stops its ability to expand further.

Bulk movement of the buccal mass

In previous studies of transilluminated juvenile *Aplysia californica*, we observed that the line connecting the jaws and the esophagus served as a fixed reference frame for overall movements of the buccal mass (Drushel et al., 1997). In the present study, we observed that the posterior part of the buccal mass was free to move relative to the jaws, and we therefore chose to use the line of the jaws as an intrinsic reference frame. In our previous studies, we observed that the overall movement of the buccal mass was relatively consistent (see fig. 4 in Drushel et al., 1997), whereas in this study we found considerable variability (Fig. 10). One reason for the difference may be that the previous studies utilized juvenile slugs that were swallowing a cut piece of seaweed that was large and stiff relative to their scale. As a consequence, their entire buccal mass was effectively held rigidly around this rod so that the esophagus was constrained to rotate together with the jaws. The large animals used in this study are swallowing a relatively soft noodle or polyethylene tube, and the posterior part of the buccal mass is free to move relative to the jaws. The movements of the posterior part of the buccal mass are likely to reflect both internal deformations and the effects of the extrinsic muscles and may, therefore, be more variable. Another possible reason for the discrepancy between results is that we were unable to visualize the foot and head borders of the animal clearly in these studies, because they are essentially transparent in MRI, and movements of these surrounding structures relative to the fixed frame of the holding capsule would also affect the angle of the jaw line.

Kinematics of the odontophore

If the odontophore were a rigid body, its net translation and rotation relative to the line of the jaws could be considered independently of its deformations and the internal movements of the radular stalk. As is clear from examination of the MR images, however, the internal expansion or contraction of the odontophore affects both the angle that its anterior edge makes with the jaw line and the movement of the point that is closest to the line of the jaws. Thus, we will consider all these movements simultaneously during each part of the swallowing cycle.

During protraction, the radular stalk translates into the odontophore (Fig. 13, right panels, *t4* period) and the odontophore becomes widest in its antero-posterior dimension (Fig. 12, left panels, *t4* period). The odontophore also undergoes its maximum anterior rotation during protraction, in part because of its antero-posterior expansion (Fig. 11, left panels, *t4* period). As the radular stalk moves into the odonotophore and the odontophore expands at the onset of protraction, the radular stalk initially rotates away from the anterior margion of the odontophore (Fig. 13, left panels, *t4* period). In each swallowing response, this is followed by a consistent rotation of the radular stalk towards the anterior margin of the odontophore, followed by a further rotation away from the anterior margin. These observations suggest that, as the odontophore moves anteriorly into the lumen of the jaws during protraction, the halves of the odontophore may be kept open by pulling the radular sac and stalk into the odontophore,

and the anterior and posterior rotation of the radular stalk relative to the anterior margin of the odontophore may reflect an additional muscular contraction that prolongs the opening phase by keeping the radular sac and stalk within the odontophore despite the constricting forces of jaw musculature.

Early in retraction, the anterior translation of the odontophore reaches its peak even though the odontophore has already begun to rotate posteriorly (Fig. 11, *t1* period; compare right and left panels), accompanied by a peak increase in its dorso-ventral length (Fig. 12, right panels, *t1* period). After the peak anterior translation, the radular stalk translates out of the odontophore (Fig. 13, right panels, *t1* period) and rotates away from the anterior edge of the odontophore (Fig. 13, left panels, *t1* period). During late retraction, there is an abrupt increase in the posterior rotation and translation of the odontophore (Fig. 11, *t1* period), which is associated with the very rapid posterior rotation of the elongated odontophore out of the jaw lumen. These observations suggest that the radula may begin closing at approximately the time of peak protraction, perhaps because of a contraction of the I4 muscles, which push the radular stalk out of the odontophore. The entire elongated structure rotates posteriorly, probably as a result of passive forces and/or activation of musculature at the interdigitation of the ventral I3 and I4 muscles (the 'hinge'). Contraction of the I3 muscles, causing the jaw lumen to squeeze down medio-laterally upon the odontophore, and the changed shape of the odontophore induce it to 'snap back' once it has rotated far enough posteriorly out of the jaw musculature (indications of the snap-back are seen in Fig. 5, frames 16–18, Figs 7E, 8E, left panels, Figs 9E, 13E, right panels, and Fig. 11E, left and right panels).

During the loss of the Γ shape, the odontophore rotates and translates backwards (Fig. 11, *t2* period) and contracts in both its dorso-ventral and antero-posterior dimensions (Fig. 12, right and left panels, *t2* period), and the radular stalk both translates into the odontophore and rotates away from its anterior edge (Fig. 13, *t2* period). If the odontophore is isovolumetric, the contraction in the dorso-ventral and antero-posterior dimensions implies that it expands in the medio-lateral dimension. This inference and the movements of the radular stalk all suggest that, at this phase, the halves of the radula are opening. Thus, the underlying mechanism of the Γ shape of the overall buccal mass is the posterior rotation of the closed radula halves and elongated odontophore into the esophagus, and the loss of the Γ shape is due to the rapid translation of the radular stalk into the odontophore as the halves of the radula open. We will refer to this rapid inward translation of the radular stalk into the odontophore as the 'collapse' of the elongated odontophore, but this term is not meant to imply that the movement is passive or that the entire structure becomes smaller in all dimensions, since it is likely to involve active forces and an expansion of the odontophore in the medio-lateral dimension.

One possible way in which the radular stalk could move into the odontophore would be if it were strongly compressed by the I2 muscle. However, the radular stalk begins to translate into the odontophore near the end of the *t1* period (Fig. 13, right panels), and the I2 muscle does not begin to shorten significantly until the middle of the *t2* phase (Fig. 7). Furthermore, studies of its activation *in vivo* suggest that it does not actively contract until the onset of the protraction phase, *t4* (see fig. 11 in Hurwitz et al., 1996) (see fig. 12 in Drushel et al., 1998). It is possible that the passive properties of I2, which are significant when it is stretched beyond $1.0 l_{mto}$, could contribute to the collapse (Yu et al., 1999). The data suggest, however, that activation of the I7 muscle could play a more significant role in moving the radular stalk into the odontophore (Evans et al., 1996).

Variability of responses and degrees of freedom in the buccal mass

Although we have focused primarily on the common features of all four sequences, which can be observed both in the individual responses and in the normalized, averaged responses, the variability among the four swallowing responses is striking. The durations of the swallows vary (swallow 1, 5.6 s; swallow 2, 6.8 s; swallow 3, 7.1 s; swallow 4, 6.5 s) and the amplitudes of the motions vary (for example, compare the anterior translation of the odontophore during the protraction period in swallow 1 with that in swallow 2, Fig. 11A,B, right traces, *t1* period). In the same animal, two swallows that immediately follow one another can vary significantly. Swallows 1 and 2 immediately follow one another in one animal, and swallows 3 and 4 immediately follow one another in a second animal. The variability in the swallowing responses may be due to the great variability observed in ingestive-like motor patterns observed in isolated buccal ganglia, even though sensory feedback is absent, and thus may be due to inherent properties of the central pattern generator for feeding; see, for example, Church and Lloyd (1994), who comment on the great variability of patterns seen in reduced preparations and even in isolated ganglia. It may also be due to the changing conditions of the food and its positioning within the buccal mass, which could strongly and rapidly modulate the feeding responses. It is known, for example, that changing the mechanical load on the buccal mass can rapidly alter neuronal responses (Hurwitz and Susswein, 1992). Finally, the variability may be due to the inherently flexible nature of the muscle and cartilage that constitute the buccal mass, which may afford a relatively large number of degrees of freedom that can be affected flexibly both by changes in neural output and by interactions with the biomechanics of food. These observations support our hypothesis that understanding the full functionality of systems with a high level of neural and biomechanical flexibility requires the simultaneous monitoring of both aspects of the system in freely behaving subjects.

We thank the Whitehall Foundation (grant M97-12 to H.J.C.) and the NSF (grant IBN-9974394 to H.J.C.; IGERT NSF 9972747) for supporting this research. We thank Greg

Sutton and two anonymous reviewers for comments on an earlier draft of this manuscript.

References

Brezina, V., Orekhova, I. V. and Weiss, K. R. (2000). Optimization of rhythmic behaviors by modulation of the neuromuscular transform. *J. Neurophysiol.* **83**, 260–279.

Cabeza, R. and Nyberg, L. (2000). Imaging cognition. II. An empirical review of 275 PET and fMRI studies. *J. Cogn. Neurosci.* **12**, 1–47.

Chiel, H. J. and Beer, R. D. (1997). The brain has a body: Adaptive behavior emerges from interactions of nervous system, body and environment. *Trends Neurosci.* **20**, 553–557.

Chiel, H. J., Neustadter, D. M., Sutton, G., Drushel, R. F. and Crago, P. E. (1999). MRI imaging and kinematic modeling of feeding responses of the buccal mass of *Aplysia californica*. *Soc. Neurosci. Abstr.* **25**, 1128.

Church, P. J., Cohen, K. P., Scott, M. L. and Kirk, M. D. (1991). Peptidergic motoneurons in the buccal ganglia of *Aplysia californica*: immunocytochemical, morphological and physiological characterizations. *J. Comp. Physiol. A* **168**, 323–336.

Church, P. J. and Lloyd, P. E. (1994). Activity of multiple identified motor neurons recorded intracellularly during evoked feedinglike motor programs in *Aplysia*. *J. Neurophysiol.* **72**, 1794–1809.

Clarys, J. P. (2000). Electromyography in sports and occupational settings: an update of its limits and possibilities. *Ergonomics* **43**, 1750–1762.

D'Esposito, M. (2000). Functional neuroimaging of cognition. *Semin. Neurol.* **20**, 487–498.

Drushel, R. F., Neustadter, D. M., Hurwitz, I., Crago, P. E. and Chiel, H. J. (1998). Kinematic models of the buccal mass of *Aplysia californica*. *J. Exp. Biol.* **201**, 1563–1583.

Drushel, R. F., Neustadter, D. M., Shallenberger, L. L., Crago, P. E. and Chiel, H. J. (1997). The kinematics of swallowing in the buccal mass of *Aplysia californica*. *J. Exp. Biol.* **200**, 735–752.

Evans, C. G. and Cropper, E. C. (1998). Proprioceptive input to feeding motor programs in *Aplysia*. *J. Neurosci.* **18**, 8016–8031.

Evans, C. G., Rosen, S., Kupfermann, I., Weiss, K. R. and Cropper, E. C. (1996). Characterization of a radula opener neuromuscular system in *Aplysia*. *J. Neurophysiol.* **76**, 1267–1281.

Grasso, R., Bianchi, L. and Lacquaniti, F. (1998). Motor patterns for human gait: backward *versus* forward locomotion. *J. Neurophysiol.* **80**, 1868–1885.

Hardy, C. J., Darrow, R. D., Pauly, J. M., Kerr, A. B., Dumoulin, C. L., Hu, B. S. and Martin, K. M. (1998). Interactive coronary MRI. *Mag. Res. Med.* **40**, 105–111.

Hatzitaki, V. and McKinley, P. (2001). Effect of single-limb inertial loading on bilateral reaching: interlimb interactions. *Exp. Brain Res.* **140**, 34–45.

Hurwitz, I., Goldstein, R. S. and Susswein, A. J. (1994). Compartmentalization of pattern-initiation and motor functions in the B31 and B32 neurons of the buccal ganglia of *Aplysia californica*. *J. Neurophysiol.* **71**, 1514–1527.

Hurwitz, I., Kupfermann, I. and Susswein, A. J. (1997). Different roles of neurons B63 and B34 that are active during the protraction phase of buccal motor programs in *Aplysia californica*. *J. Neurophysiol.* **75**, 1327–1344.

Hurwitz, I., Neustadter, D., Morton, D. W., Chiel, H. J. and Susswein, A. J. (1996). Activity patterns of the B31/B32 pattern initiators innervating the I2 muscle of the buccal mass during normal feeding movements in *Aplysia californica*. *J. Neurophysiol.* **75**, 1309–1326.

Hurwitz, I. and Susswein, A. (1992). Adaptation of feeding sequences in *Aplysia oculifera* to changes in the load and width of food. *J. Exp. Biol.* **166**, 215–235.

Hurwitz, I. and Susswein, A. J. (1996). B64, a newly-identified central pattern generator element producing a phase switch from protraction to retraction in buccal motor programs of *Aplysia californica*. *J. Neurophysiol.* **75**, 1327–1344.

Jing, J. and Weiss, K. R. (2001). Neural mechanisms of motor program switching in *Aplysia*. *J. Neurosci.* **21**, 7349–7362.

Kandel, E. R. and Pittenger, C. (1999). The past, the future and the biology of memory storage. *Phil. Trans. R. Soc. Lond. B* **354**, 2027–2052.

Katz, P. S. and Frost, W. N. (1996). Intrinsic neuromodulation: altering neuronal circuits from within. *Trends Neurosci.* **19**, 54–61.

Kirk, M. D. (1989). Premotor neurons in the feeding system of *Aplysia californica*. *J. Neurobiol.* **20**, 497–512.

Kuhtz-Buschbeck, J. P., Ehrsoon, H. H. and Forssberg, H. (2001). Human brain activity in the control of fine static precision grip forces: an fMRI study. *Eur J. Neurosci.* **14**, 382–390.

Kupfermann, I. (1974). Feeding behavior in *Aplysia*: A simple system for the study of motivation. *Behav. Biol.* **10**, 1–26.

Kupfermann, I., Brezina, V., Cropper, E. C., Deodhar, D., Probst, W. C., Rosen, S. C., Vilim, F. S. and Weiss, K. R. (1998). Reconfiguration of the peripheral plant during various forms of feeding behaviors in the mollusc *Aplysia*. In *Neurons, Networks and Motor Behavior* (ed. P. S. G. Stein, S. Grillner, A. I. Selverston and D. G. Stuart), pp. 217–222. Cambridge, MA: The MIT Press.

Morgan, P. T., Perrins, R., Lloyd, P. E. and Weiss, K. R. (2000). Intrinsic and extrinsic modulation of a single central pattern generating circuit. *J. Neurophysiol.* **84**, 1186–1193.

Morton, D. W. and Chiel, H. J. (1993). The timing of activity in motor neurons that produce radula movements distinguishes ingestion from rejection in *Aplysia*. *J. Comp. Physiol. A* **173**, 519–536.

Murphy, A. D. (2001). The neuronal basis of feeding in the snail, *Helisoma*, with comparisons to selected gastropods. *Prog. Neurobiol.* **63**, 383–408.

Neustadter, D. M., Drushel, R. F., Crago, P. E. and Chiel, H. J. (2001). A 3-dimensional model of the odontophore of *Aplysia* throughout a swallowing cycle. *Soc. Neurosci. Abstr.* **27**, 943.7.

Orekhova, I. V., Jing, J., Brezina, V., DiCaprio, R. A., Weiss, K. R. and Cropper, E. C. (2001). Sonometric measurements of motor-neuron-evoked movements of an internal feeding structure (the radula) in *Aplysia*. *J. Neurophysiol.* **86**, 1057–1061.

Rosen, S. C., Teyke, T., Miller, M. W., Weiss, K. R. and Kupfermann, I. (1991). Identification and characterization of cerebral-to-buccal interneurons implicated in the control of motor programs associated with feeding in *Aplysia*. *J. Neurosci.* **11**, 3630–3655.

Selverston, A. I. (1985). *Model Neural Networks and Behavior*. New York: Plenum Press.

Silva, A. J., Kogan, J. H., Frankland, P. W. and Kida, S. (1998). CREB and memory. *Annu. Rev. Neurosci.* **21**, 127–148.

Stein, P. S. G., Grillner, S., Selverston, A. I. and Stuart, D. G. (1997). *Neurons, Networks and Motor Behavior*. Cambridge, MA: MIT Press.

Susswein, A. J. and Byrne, J. H. (1988). Identification and characterization of neurons initiating patterned neural activity in the buccal ganglia of *Aplysia*. *J. Neurosci.* **8**, 2049–2061.

Sutton, G. P., Drushel, R. F., Neustadter, D. M., Crago, P. E. and Chiel, H. J. (2000). A kinematic model of *Aplysia* swallowing based on MRI imaging. *Soc. Neurosci. Abstr.* **26**, 943.8.

Weiss, K. R., Brezina, V., Cropper, E. C., Hooper, S. L., Miller, M. W., Probst, W. C., Vilim, F. S. and Kupfermann, I. (1992). Peptidergic co-transmission in *Aplysia*: Functional implications for rhythmic behaviors. *Experientia* **48**, 456–463.

Yu, S.-Y., Crago, P. E. and Chiel, H. J. (1999). Biomechanical properties and a kinetic simulation model of the smooth muscle I2 in the buccal mass of *Aplysia*. *Biol. Cybern.* **81**, 505–513.